Metabolic Adaptation of Macrophages as Mechanism of Defense against Crystalline Silica

Antonella Marrocco,* Krystin Frawley,* Linda L. Pearce,* James Peterson,* James P. O'Brien,† Steven J. Mullett,†,‡ Stacy G. Wendell,†,‡,§ Claudette M. St Croix,¶ Steven E. Mischler,* and Luis A. Ortiz*

Silicosis is a lethal pneumoconiosis for which no therapy is available. Silicosis is a global threat, and more than 2.2 million people per year are exposed to silica in the United States. The initial response to silica is mediated by innate immunity. Phagocytosis of silica particles by macrophages is followed by recruitment of mitochondria to phagosomes, generation of mitochondrial reactive oxygen species, and cytokine (IL-1β, TNF-α, IFN-β) release. In contrast with LPS, the metabolic remodeling of silica-exposed macrophages is unclear. This study contrasts mitochondrial and metabolic alterations induced by LPS and silica on macrophages and correlates them with macrophage viability and cytokine production, which are central to the pathogenesis of silicosis. Using high-resolution respirometer and liquid chromatography–high-resolution mass spectrometry, we determined the effects of silica and LPS on mitochondrial respiration and determined changes in central carbon metabolism of murine macrophage cell lines RAW 264.7 and IC-21. We show that silica induces metabolic reprogramming of macrophages. Silica, as well as LPS, enhances glucose uptake and increases aerobic glycolysis in macrophages. In contrast with LPS, silica affects mitochondria respiration, reducing complex I and enhancing complex II activity, to sustain cell viability. These mitochondrial alterations are associated in silica, but not in LPS-exposed macrophages, with reductions of tricarboxylic acid cycle intermediates, including succinate, itaconate, glutamate, and glutamine. Furthermore, in contrast with LPS, these silica-induced metabolic adaptations do not correlate with IL-1β or TNF-α production, but with the suppressed release of IFN-β. Our data highlight the importance of complex II activity and tricarboxylic acid cycle remodeling to macrophage survival and cytokine-mediated inflammation in silicosis. ***The Journal of Immunology*****, 2021, 207: 1627–1640.**

Crystalline silica is one of the most abundant minerals on Earth. More than 230 million individuals around the world and more than 2 million workers in the United States, predominantly in construction and mining occupations, are exposed to silica every year (1–3). Inhalation of crystalline silica leads to the development of silicosis, a progressive pneumoconiosis characterized by lung inflammation and fibrosis, for which no specific therapy is available. Silicosis is associated with an increased risk for tuberculosis, lung cancer, chronic obstructive pulmonary disease, kidney disease, and autoimmune disease, and these health risks remain increased even after silica exposure has ceased (2, 4–6).

Macrophages are fundamental to the pathogenesis of silicosis. Similar to live bacteria, silica particles are phagocytosed by macrophages into phagosomes. Subsequently, macrophages activate pattern recognition receptors and the NLRP3 inflammasome, and release cytokines, such as IL-1β, TNF-α, and IFNs, key mediators of the pathogenesis of silicosis (7). In contrast with bacteria, silica particles cannot be degraded, and the persistent activation results in an increased NADPH oxidase activation and mitochondrial reactive oxygen species (ROS) production that ultimately leads to macrophage cell death and release of silica particles that perpetuate inflammation (2, 8–10). Activated macrophages exhibit altered immunometabolism, intracellular metabolic changes that govern immune effector mechanisms, such as cytokine secretion. For example, LPS-stimulated macrophages demonstrate enhanced glycolysis and increased secretion of IL-1β and TNF-α (11–13). Inhibiting glycolysis or blocking succinate dehydrogenase (SDH), an enzyme that links glycolysis and the electron transport chain (ETC), in LPS-stimulated macrophages inhibits IL-1β, but not TNF-α, proving that the metabolic pathway is specifically involved in cytokine production (11).

*Department of Environmental and Occupational Health, Graduate School of Public Health at the University of Pittsburgh, Pittsburgh, PA; †Department of Pharmacology and Chemical Biology, University of Pittsburgh, Pittsburgh, PA; ‡Health Sciences Metabolomics and Lipidomics Core, University of Pittsburgh, Pittsburgh, PA; §Clinical Translational Science Institute, University of Pittsburgh, Pittsburgh, PA; and ¶Department of Cell Biology, University of Pittsburgh, Pittsburgh, PA

ORCIDs: 0000-0002-6515-1980 (A.M.); 0000-0002-7300-5887 (J.P.); 0000-0003-2784-6906 (J.P.O.); 0000-0001-9083-6933 (S.G.W.); 0000-0001-5360-2855 (S.E.M.); 0000-0003-4510-7066 (L.A.O.).

Received for publication May 29, 2020. Accepted for publication July 8, 2021.

This work was supported by the Department of Health and Human Services (HHS), National Institutes of Health (NIH), National Heart, Lung, and Blood Institute (NHLBI) (grants 1R01HL114795 and 1R01HL110344 to L.A.O.); HHS, NIH, NIH Office of the Director (grant S10OD023402 to S.G.W.); and HHS, NIH, National Institute of Environmental Health Sciences (NIEHS) (grant ES015859 to L.A.O.).

Address correspondence and reprint requests to Dr. Luis A. Ortiz, Division of Occupational and Environmental Health, Graduate School of Public Health at the University of Pittsburgh, 130 De Soto Street, Pittsburgh, PA 15261. E-mail address: lao1@pitt.edu

The online version of this article contains supplemental material.

Abbreviations used in this article: BMDM, bone marrow-derived macrophage; cat#, catalog number; CCCP, carbonyl cyanide *m*-chlorophenyl hydrazone; CI, complex I; CII, complex II; ΔCt, Δ cycle threshold; Ecsit, evolutionarily conserved signaling intermediate in Toll pathway; ETC, electron transport chain; H_2O_2, hydrogen peroxide; LC-HRMS, liquid chromatography–high-resolution mass spectrometry; LDH, lactate dehydrogenase; MIMOSA, mass isotopomer multiordinate spectral analysis; PI, propidium iodide; ROS, reactive oxygen species; SDH, succinate dehydrogenase; SUIT, substrate-uncoupler-inhibitor titration; TAC, tricarboxylic acid cycle; TEM, transmission electron microscopy.

Despite decades of research, the nature of the immunometabolic response induced by silica in macrophages, its contribution to cytokine specification, and the pathogenesis of silicosis are not well understood. In addition, recent studies indicate that the macrophages' ontogeny, resident in the lung versus recruited from bone marrow in response to injury, determines differences in the in vivo metabolic response to LPS stimuli (14–16). Therefore, as an initial step to characterize the difference between the silica- and LPS-induced metabolic effects on macrophages, we adopted an in vitro system using well-characterized macrophage cell lines that differ on the cytokine production in response to these agents, and applied state-of-the-art techniques, such as high-resolution respirometry and liquid chromatography–high-resolution mass spectrometry (LC-HRMS), to determine the effects of silica on mitochondrial respiration and the changes in central carbon metabolism of silica-exposed macrophages. Specifically, we characterized the metabolic reprogramming of silica-stimulated macrophages, in terms of alteration in glycolysis, tricarboxylic acid cycle (TAC), mitochondrial respiration, and ETC activity, to correlate their contribution to cytokine specification. Using macrophage cell lines, we reported significant differences in immunometabolism in the macrophages' response to silica and LPS. We found that, similar to LPS exposure, silica increases glucose uptake and enhances glycolysis in macrophages. In contrast with LPS, which induces accumulation of TAC intermediates such as citrate, succinate, and itaconate, silica negatively affects the TAC activity, reducing the intracellular amount of TAC intermediates succinate and itaconate to less than control levels. Silica also induces specific ETC adaptations: enhanced mitochondrial complex II (CII) activity and downregulation of mitochondrial complex I (CI) activity via reductions of the CI-specific protein *Ecsit* (evolutionarily conserved signaling intermediate in Toll pathway), which are required for macrophage survival to silica-induced cytotoxicity. These metabolic responses correlated with the observed differences in macrophage production of inflammatory cytokines in response to LPS and silica. Thus, although RAW 264.7 macrophages enhanced IL-1β and TNF-α production in response to LPS or silica, only LPS-stimulated RAW 264.7 macrophages exhibited HIF-1α stabilization under normoxic conditions, activation of the NLRP3 inflammasome, and malonylation of GAPDH in a time-related manner that preceded the release of IL-1β and TNF-α. In addition, we observed differences in the RAW 264.7 macrophages accumulation of itaconate that correlate, inversely, with the transcription and release of IFN-β in response to LPS or silica. Despite intrinsic limitations associated with in vitro studies and the use of murine macrophages cell lines, the present studies provide valuable information as to how metabolic pathways determine macrophage immune metabolism in response to silica exposure. Further studies to determine therapeutic targets are warranted to investigate macrophage immunometabolic responses to silica in vivo.

Materials and Methods

Cell culture

The mouse macrophage cell lines RAW 264.7 and IC-21 were purchased from the American Type Culture Collection (Rockville, MD) and were cultured in DMEM (Life Technologies BRL, Rockville, MD) or RPMI 1640 (ATCC, Rockville, MD), respectively, supplemented with 10% FBS, 100 U/ml penicillin G, and 100 mg/ml streptomycin and grown at 37°C in 5% CO_2.

Silica particles, Abs, and reagents

Crystalline silica was isolated from environmentally relevant sources and characterized at the National Institute of Occupational Safety and Health (NIOSH, Pittsburgh, PA) using a multicyclone sampling array as previously described (10, 17). α-Quartz (average size, 1.7 μm) was also obtained from U.S. Silica (Berkeley Springs, WV). Particles were subjected to sedimentation, according to Stokes law, acid hydrolyzed, and baked overnight (200°C, 16 h) to inactivate endotoxin contamination.

Primary Abs. Anti–HIF-1α (catalog number [cat#] NB100-449) and anti-GAPDH loading control (cat# MA5-15738) were obtained from Thermo Fisher; Total OXPHOS Rodent WB Ab mixture (cat# ab110413) and anti-*Ecsit* Ab (cat# ab21288) from Abcam; anti–IL-1β/IL-1F2 Ab (cat# AF-201-NA) from R&D System; anti–caspase-1 p10 (M-20) (cat# SC-514) and A/G plus agarose beads (cat# sc-2003) and normal mouse IgG (cat# sc-2025) from Santa Cruz Biotechnology; anti–b-actin (cat# 4967) from Cell Signaling Technology; anti–malonyl lysine (cat# PTM-901) from PTM Biolabs; and anti-GAPDH (cat# MAB374) from EMO Millipore USA.

Secondary Abs. Anti-goat IgG (cat# ab6741) was from Abcam; anti-mouse IgG HRP-linked Ab (cat#7076) and anti-rabbit IgG HRP-linked Ab (cat# 7074S) from Cell Signaling; ATP Synthase (cat# MA1-930) and anti-mouse Alexa 488 (cat# A11029) from Invitrogen; and anti-rabbit Cy3 (cat# 111-164-144) from Jackson ImmunoResearch.

LPSs from *Escherichia coli* 0111:B4 (cat# L4391-1MG), L-lactate dehydrogenase (L-LDH) from rabbit muscle (cat# 10127230001), and sodium L-lactate (cat# 71718) were purchased from Millipore-Sigma (St. Louis, MO, USA).

Pierce RIPA Buffer (cat# PI89900), Halt Protease and Phosphatase Inhibitor, and Propidium Iodide 1.0 mg/ml Solution in Water (cat# P3566) were from Thermo Fisher. The D-glucose (U-13C6, 99%, cat# CLM-1396-0) was purchased from Cambridge Isotope Laboratories (Andover, MA). Annexin V-FITC Apoptosis Kit Plus (cat# K201-100) was purchased from Biovision.

Detection of cell death

Cell death was analyzed by evaluating (flow cytometry) Annexin V binding and the exclusion of propidium iodide (PI) by macrophages, as previously described (18).

LDH assay

LDH in the supernatant of exposed cells was measured using a commercial LDH release assay (TOX7; Sigma-Aldrich) according to the manufacturer's instructions. The absorbance was measured spectrophotometrically at a wavelength of 490 nm, using Cytation 5 Cell Imaging Multi-Mode Reader BioTek.

Lactate assay

Lactate concentration in the supernatant of exposed cells was assessed using a modification of the commercially available lactate assay (TOX7; Sigma-Aldrich). The reaction is based on the oxidation of lactate by LDH. Cell supernatant was incubated with an equal volume of LDH (final concentration [f.c.], 1 M), 1× LDH assay cofactor preparation, and LDH Assay Dye Solution (cat# L2277). Absorbance was acquired spectrophotometrically at a wavelength of 490 nm, using Cytation 5 Cell Imaging Multi-Mode Reader BioTek.

ETC assays

Respirometric experiments. An Oxygraph O2k Polarographic instrument (Oroboros Instruments, Innsbruck, Austria), equipped with a Clark-type electrode for high-resolution respirometry, was used to measure oxygen fluxes and concentrations. DMEM without glucose (2.1 ml) was added to each chamber and equilibrated for 20 min before the addition of cell suspension (2.5×10^6cells/ml) (prepared as described earlier) into the Oxygraph chambers (sealed from the atmosphere) at 37°C. Oxygen turnover was examined by the addition of succinate (f.c., 10 mM).

Substrate-uncoupler-inhibitor titration assay. Substrate-uncoupler-inhibitor titration (SUIT) protocol was used for the analysis of oxidative phosphorylation, to study respiratory control in a sequence of coupling and pathway control states induced by multiple titrations. After equilibration of the cells into the chamber, the substrates, inhibitors, or uncoupler was added according to the following protocol: rotenone (f.c., 0.5 μM) to inhibit CI; succinate (f.c., 10 mM) to stimulate CII; ADP (f.c., 1 mM) to measure the total respiratory capacity; carbonyl cyanide *m*-chlorophenyl hydrazone (CCCP; f.c., 0.05 μM) to determine the state of coupling of complexes III, IV, and V; and antimycin A (f.c., 2.5 μM) to inhibit complex III (Sigma-Aldrich). Hydrogen peroxide (H_2O_2) flux was assessed simultaneously using the H_2O_2-sensitive probe Amplex UltraRed, by the addition of Amplex Red (f.c., 10 μM) and HRP (f.c., 1 U/ml) (Sigma-Aldrich) following the variation of the resorufin concentration while performing the SUIT assay protocol. Additions were made by gas-tight syringe into the sealed Oxygraph chambers. Respirometric data analysis was carried out with DatLab 7 software provided by Oroboros.

CI assay

Mitochondrial CI activity was measured spectrophotometrically (DU-530; Beckman Coulter). Mitochondrial pellets were lysed in 0.05 mM potassium/phosphate buffer (0.05 mM, pH 8) containing NADH (10.0 mM),

$K_3Fe(CN)_6$ (25 mM), a phospholipid supplement (0.005% *n*-dodecyl-β-D-maltopyranoside from Anatrace), antimycin A (2.5 mM), and 320 μg protein from the cell pellet by following the oxidation of NADH at 420 nm initiated by $K_3Fe(CN)_6$ at 30°C–38°C. Data were acquired for 100 s after initiation of the reaction.

CII assay

Mitochondrial CII activity was measured spectrophotometrically (DU-530; Beckman Coulter), using a modification of the commercially available Complex II Enzyme Activity Microplate Assay Kit (colorimetric) (cat# ab109908; Abcam). Proteins were extracted in PBS and detergent, then lysed in CII activity buffer, lipid/phospholipid mix, 2,6-dichloroindophenol and Ubiquinone-2, and succinate as provided by the kit and 300 μg protein from the cell pellet. The reaction was followed by measuring the decrease in absorbance at 600 nm for 100 s at room temperature. The activity of CII was expressed as mAbs per minute per microgram of protein (mAbs/min/μg protein).

Protein immunoprecipitation and Western blotting

A total of 10×10^6 cells/condition were lysed with 1 ml of ice-cold Pierce RIPA Buffer with protease inhibitors and disrupted by repeated aspiration through a 21-gauge needle. Protein concentration was measured using BCA protein assay (cat# 23225; Thermo Fisher) and normalized across samples before immunoprecipitation. A total of 500 μl lysate was precleared with 1.0 μg of appropriate control IgG (normal mouse) and 20 μl A/G PLUS agarose for 30 min at 4°C. For GAPDH immunoprecipitation, 100–500 μg of total cellular protein was incubated with 2 μg of primary Ab for 1 h at 4°C, then 20 μl of A/G beads was added overnight and incubated overnight at 4°C on a rocker platform. Immunoprecipitates were collected by centrifugation at 1000 × *g* for 5 min at 4°C, the liquid was removed, and the pellets were washed four times with PBS. Immune complexes were eluted by adding 40 μl of 1× electrophoresis sample buffer, boiled for 5 min at 95°C, and analyzed by SDS-PAGE.

Protein samples from cultured cells were prepared by lysis with RIPA buffer with protease inhibitors. Protein concentration was determined using the BCA protein assay (cat# 23225; Thermo Fisher). A total of 20–50 μg of protein samples was separated by SDS-PAGE and transferred onto a polyvinylidene difluoride membrane via iBlot (Invitrogen) transfer. Membranes were blocked in 5% nonfat milk and incubated with primary Abs and HRP-conjugated secondary Abs. Membranes were probed with the respective Abs and visualized using SuperSignal West Femto Maximum sensitivity substrate (cat# 34095; Thermo Scientific) and Amersham Imager 600.

Immunofluorescence staining

RAW 264.7 macrophages were plated on coverslips, allowed to grow overnight, and stimulated with LPS (1 ng/ml) or silica (50 μg/cm^2) with or without priming with LPS (1 ng/ml) for 24 h. Cells were fixed with 2% paraformaldehyde in PBS for 15 min at 4°C. Cells were permeabilized with 0.1% Triton X-100 in PBS with 0.5% BSA for 15 min. Cells were blocked with 2% normal goat serum for 45 min and stained overnight for primaries for ECSIT (ab21288; Abcam) with ATP synthase (MA1-930; Invitrogen) and HIF-1 α (NB100-449; Novus) with ATP synthase. Corresponding secondary Abs anti-rabbit Cy3 (111-164-144; Jackson ImmunoResearch) and anti-mouse Alexa 488 (A11029; Invitrogen) were added for 1 h. Nuclei were stained with Hoechst (B2883; Sigma) 1 mg/100 ml dH_2O for 1 min, washed in PBS, and mounted in Gelvatol. Large area scan images were obtained on Nikon A1 confocal microscope with NIS Elements v4.4 at 60× magnification.

Isolation of mitochondria

Mitochondria were isolated from control, silica, or silica plus LPS-stimulated RAW 264.7 macrophages using a Mitochondria Isolation Kit for Cultured Cells (cat# 89874; Thermo Fisher) following the manufacturer's instructions.

ELISA

Cytokines concentration in cell supernatants was measured using ELISA kits for mouse IL-1β, TNF-α, and IFN-β, Mouse IL-1β ELISA MAX Standard (cat# 432601; BioLegend) or Mouse TNF-α ELISA MAX Standard (cat#430902; BioLegend), according to the manufacturer's instructions. Mouse IFN-β DuoSet ELISA (cat# DY8234-05) was purchased by Bio-Techne. OD values were measured at a wavelength of 450 nm, using Cytation 5 Cell Imaging Multi-Mode Reader BioTek.

RNA analysis

Total cellular RNA was isolated from cells using TRIzol reagent (Invitrogen) following the manufacturer's instructions. The concentration of total RNA was quantified at an absorbance of 260 nm. Real-time qPCR was performed on RNA by an RT-PCR using TaqMan RNA-to Ct 1-Step Kit (Applied Biosystems), according to the manufacturer's instructions, using 500 ng of RNA as a starting material, in a total reaction volume of 10 μL. PCR conditions were as follows: 15 min at 48°C, 10 min at 95°C, followed by 40 cycles with 15 s at 95°C and 1 min at 60°C in the ABI 7300 real-time PCR system. The qRT-PCR was performed on RNA using probes specific for TNF-α (Mm00443258_m1), IL-1β (Mm00434228_m1), and IFN-β (Mm00439552_s1) (Thermo Fisher). The GUSB (Mm01197698_m1) or GAPDH (Mm9999915_g1) (Thermo Fisher) was used for normalization. The Δ cycle threshold (ΔCt) was calculated by subtracting the Ct of GUSB or GAPDH from the Ct of the gene of interest. ΔΔCt was calculated by subtracting the ΔCt of the reference sample from ΔCt of control sample. Fold change was generated using the equation $2^{-\Delta\Delta}$.

Metabolic assay

Stable isotope labeling. [^{13}C] tracer analysis and high-resolution mass spectrometry were used to discern subtle shifts in energy substrate metabolism in specific reactions through the detection and quantification of metabolite isotopologues. RAW 264.7 macrophages (1×10^6/well in six-well plate) were activated with LPS (10 ng/ml) or silica (50 μg/cm^2) dissolved in DMEM without glucose, supplemented with ^{12}C- or U[^{13}C]-labeled glucose (4.5 mg/l), 5% FBS dialyzed. Experiments were conducted (n = 6/condition). Controls included vehicle control and the ^{12}C glucose control for each treatment condition.

Untargeted LC-HRMS. **Sample preparation.** Metabolic quenching and polar metabolite extraction were performed using ice-cold 80% methanol/0.1% formic acid at a ratio of 500 μL per 1×10^6 adherent cells. An internal standard mix containing (D3)-creatinine and (D3)-alanine, (D4)-taurine, and (D3)-lactate (Sigma-Aldrich) was added to the sample lysates at an f.c. of 100 μM. After 3 min of vortexing, the supernatant was cleared of protein by centrifugation at 16,000 × *g*. Cleared supernatant (3 μL) was subjected to online separation and analysis.

LC-HRMS method. Analyses were performed by untargeted LC-HRMS. In brief, samples were injected via a Thermo Vanquish UHPLC and separated over a reversed-phase Thermo HyperCarb porous graphite column (2.1 × 100 mm, 3-μm particle size) maintained at 55°C. For the 20-min LC gradient, the mobile phase consisted of the following: solvent A (water/0.1% formic acid) and solvent B (acetonitrile/0.1% formic acid). The gradient was the following: 0–1 min 1% B, increasing to 15% B over 5 min, increasing to 98% B over 5 min, and held at 98% B for 5 min before equilibration to starting conditions. The Thermo ID-X tribrid mass spectrometer was operated in positive and negative ion mode, scanning in full MS mode (two microscans) from 100 to 800 *m/z* at 70,000 resolution with an automatic gain control target of 2×10^5. Source ionization setting was 3.0 kV/2.4vkV spray voltage for positive and negative modes, respectively. Source gas parameters were 45 sheath gas, 12 auxiliary gas at 320°C, and 8 sweep gas. Calibration was performed before analysis using the Pierce FlexMix Ion Calibration Solution (Thermo Fisher Scientific). Alignment and peak area integration were then extracted manually using Quan Browser (Xcalibur ver. 2.7; Thermo Fisher). Atomic percent enrichment was calculated using the established mass isotopomer multiordinate spectral analysis (MIMOSA) method to remove the natural [^{13}C] abundance background (19).

Transmission electron microscopy analysis

At 1, 2, and 4 h after exposure, cells were fixed in 2.5% glutaraldehyde in PBS and postfixed in 1% osmium tetroxide in PBS, dehydrated through a graded series of alcohols, and embedded in Epon (Energy Beam Sciences, Agawam, MA). Thin (70-nm) sections were cut using a Reichert Ultracut S (Leica, Deerborn, MI), mounted on 200-mesh copper grids, and counterstained with 2% aqueous uranyl acetate for 7 min and 1% aqueous lead citrate for 2 min. Observation was with a JEOL 1011 transmission electron microscope (Peabody, MA). After transmission electron microscopy (TEM), images were collected; they were formatted using Adobe Photoshop for brightness and contrast. In addition, during slide preparation, a silica particle could create stretching in the Epon resin during the slicing sequence, and when stretching was severe, the silica particle could fall out of the resin. During TEM imaging, any areas where the silica particles fell out will show as bright white, causing difficulty in image focusing. These images were corrected by recoloring the white areas back to the color of the silica particles. Importantly, this may result in a slight increase in the silica particle size for the areas that were recolored. In the images at higher magnification, these areas are labeled.

Statistics

The results are presented as mean ± SD from at least three experiments, and statistical analyses were performed using the Student *t* test or one-way ANOVA corrected for multiple comparisons, using Prism software (version

7; GraphPad Software). The statistical significance of differences was set at $p < 0.05$.

Results

Crystalline silica and low-dose LPS enhance the glycolysis without affecting macrophage viability

To study the effect of silica on glycolysis, we used RAW 264.7 macrophages, which we have previously shown release high concentrations of TNF-α and IL-1β in response to silica while experiencing low cytotoxicity to a wide range of concentrations of silica particles (8). Using these macrophages, we show that both low-dose LPS (1 ng/ml), which did not alter macrophage viability, and high-dose concentrations (10 ng/ml), which induced a significant amount of cell necrosis with associated release of LDH, were as effective as noncytotoxic doses of silica (ranging from 10 to 50 μg/cm^2) in promoting the release of a significant amount of lactate in RAW 264.7 macrophages over a period of 24 h (Fig. 1A). Addition of silica to low-dose LPS-primed RAW 264.7 macrophages induced a significantly greater increase in the release of lactate compared with cells treated with silica or LPS alone (Fig. 1B, 1C). Under these experimental conditions, RAW 264.7 macrophages exposed to silica (50 μg/cm^2) or LPS (10 ng/ml) alone experienced low levels of necrosis, and less than 30% of the cells exhibited PI uptake 24 h after exposure (Fig. 1D, 1E). In contrast, the combination of silica and LPS induced significant necrosis, with 70% of the cells taking up PI 24 h after exposure (Fig. 1D, 1E).

Silica remodels ETC complexes activity

In response to live bacteria, but not LPS, macrophages experience mitochondrial respiratory change adaptations that contribute to their antimicrobial response (12). These effects require the phagocytosis of bacteria into a phagosome, are metabolically demanding, and contribute to cytokine production (12). Similar to bacteria, silica particles are phagocytosed by macrophages into phagosomes and attract mitochondria to these organelles (Supplemental Fig. 1) (10). Using a high-resolution respirometer, we evaluated the effects of silica on mitochondrial respiration, as well as the activity and integrity of the ETC in RAW 264.7 macrophages. To evaluate the contribution of CII in the respiration of silica-activated macrophages, LPS- or silica-exposed RAW 264.7 macrophages were stimulated with succinate, the CII substrate, and the oxygen flux was subsequently recorded. When healthy untreated cells were stimulated with succinate, the oxygen flux through the ETC physiologically increased (Fig. 2A). This physiological response, identified 2 h after exposure, was significantly augmented in cells treated with silica, and although it peaked 6 h after exposure when the oxygen flux increased 3-fold, it lasted for the 24-h experiment (2 h: 2.265 ± 0.04950, $p < 0.0001$; 4 h: 2.265 ± 0.03536, $p < 0.0001$; 6 h: 2.850 ± 0.7212, $p < 0.0001$; 24 h: 2.095 ± 0.1344, $p < 0.0001$). In contrast, RAW 264.7 macrophages exposed to LPS showed only a modest, although significant, and transitory, achieving maximal response by 6 h (1.929 ± 0.06757, $p < 0.01$), increase in mitochondrial respiration in response to succinate, even in the presence of silica (Fig. 2B). LPS/silica

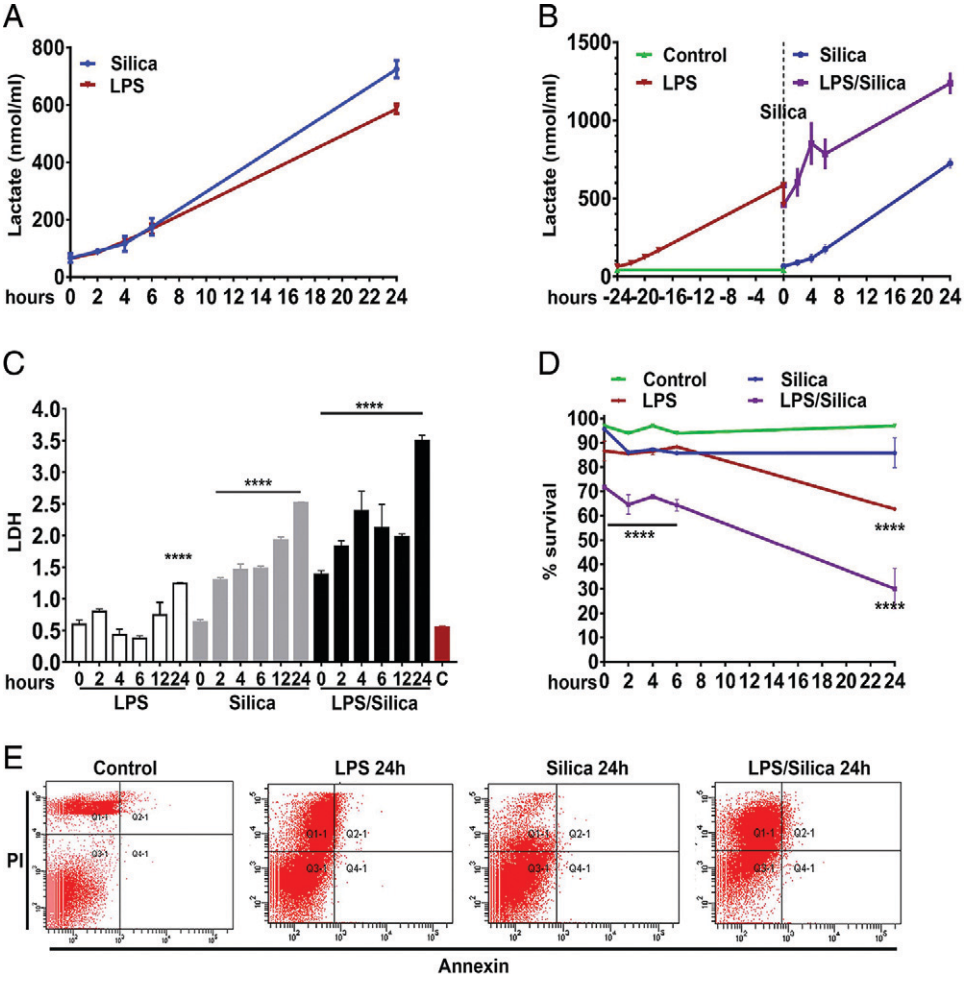

FIGURE 1. Crystalline silica and low-dose LPS enhance glycolysis without affecting macrophage viability. RAW 264.7 macrophages were exposed to LPS (1 ng/ml) or silica (50 μg/cm^2) or primed with LPS (1 ng/ml for 24 h) and then exposed to silica (50 μg/cm^2) and studied at time points of T0, 2, 4, 6, and 24 h. The cell supernatants were examined for the concentration of released (**A** and **B**) lactate and (**C**) LDH. (**D** and **E**) Annexin V and PI were used to analyze cell survival by flow cytometry: (D) graph summarizing the survival of cells treated with LPS (10 ng/ml) or silica (50 μg/cm^2) or primed with LPS (1 ng/ml for 24 h) and then exposed to silica (50 μg/cm^2). (E) Gating strategy to differentiate cell death by early apoptosis (Annexin V^+PI^-), late apoptosis (Annexin V^+PI^+), or necrosis (Annexin V^-/PI). Data were normalized by equalizing the protein concentration or equating the actual number of live cells used to perform the experiments. $n = 3$; ****$p < 0.0001$

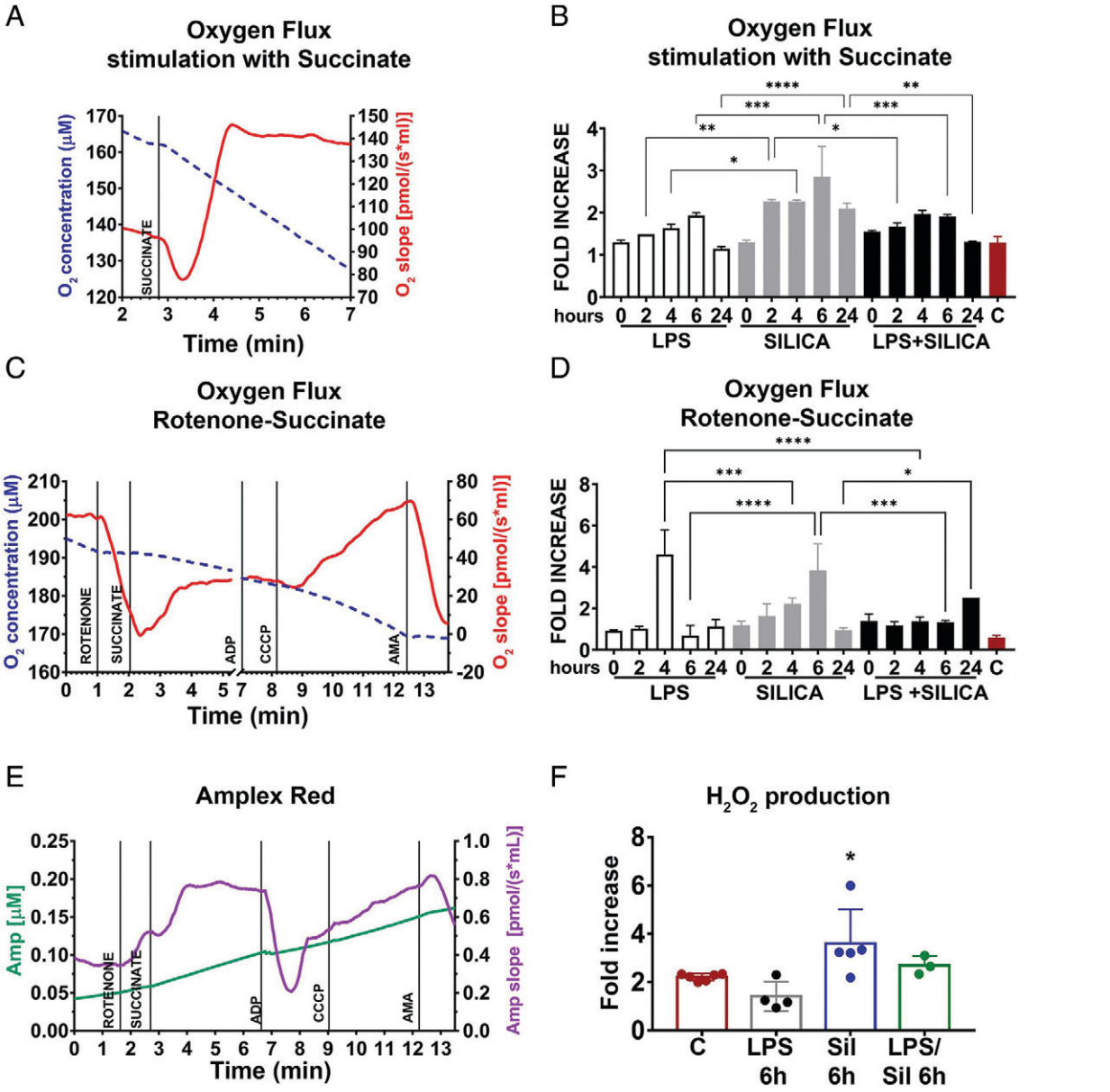

FIGURE 2. Silica remodels ETC complexes activity. RAW 264.7 macrophages were exposed to LPS (1 ng/ml) or silica (50 μg/cm^2) or primed with LPS (1 ng/ml for 24 h) and then exposed to silica (50 μg/cm^2) at time points of T0, 2, 4, 6, and 24 h. RAW 264.7 macrophages (5×10^6/chamber) were allowed to equilibrate in the chamber for ∼10 min before measuring oxygen flow. Default respirometric settings of block temperature 37°C, stir bar speed 400 rpm, and data recording every 2 s were used. Oxygen turnover (oxygen concentration, left *y*-axis; oxygen flux, right *y*-axis) by treated RAW 264.7 macrophages was followed after addition of (**A**) succinate (final concentration [f.c.], 10 mM) or (**C**) rotenone (f.c., 0.5 μM), succinate (f.c., 10 mM), ADP (f.c., 2.5 mM), CCCP (f.c., 0.05 μM), and antimycin A (f.c., 2.5 μM). After the addition of each compound, cells were allowed to come to equilibrium. Because the variation in oxygen concentration (broken traces) is difficult to appreciate because it is very little, the slope of the oxygen concentration is also shown (solid trace), which represents the negative derivative of the oxygen concentration. Variations in oxygen flux for each condition were measured as a ratio between the value of the O_2 slope at the equilibrium after treatment with succinate (with or without prior inhibition of complex I with rotenone), and the value of O_2 slope at the baseline. (**B**) Fold increase of oxygen flux after stimulation with succinate. (**D**) Fold increase of oxygen flux after the inhibition of CI with rotenone and stimulation of CII with succinate. (**E**) The production of H_2O_2 has been assessed following the slope (purple trace) of the concentration of the fluorescent Amplex Red assay product resorufin (green trace) while performing a SUIT assay protocol (see *Substrate-uncoupler-inhibitor titration assay.*). Variations in H_2O_2 for each condition were measured as the ratio between the value of the slope at the equilibrium after the inhibition of CI with rotenone and the stimulation of CII with succinate, the slope at the equilibrium at the baseline. (**F**) Fold increase of H_2O_2 production after inhibition of CI with rotenone and stimulation of CII with succinate. $n = 4$; *$p < 0.05$, **$p < 0.01$, ***$p < 0.001$, ****$p < 0.0001$ versus control. Sil, silica.

treatment induced a statistically significant increase in oxygen consumption only after 4–6 h after exposure (4 h: 1.970 ± 0.08485, $p < 0.01$; 6 h: 1.905 ± 0.04950, $p < 0.01$) (Fig. 2B). The comparison between LPS and silica treatment at every time point during the study confirmed that silica induced a statistically significantly greater increase oxygen consumption at 2 h (LPS versus silica: 1.486 ± 0.0005459 versus 2.265 ± 0.04950, $p < 0.01$), 4 h (LPS versus silica: 1.634 ± 0.08633 versus 2.265 ± 0.03536, $p < 0.05$), 6 h (LPS versus silica: 1.929 ± 0.06757 versus 2.850 ± 0.7212, $p < 0.001$), and 24 h (LPS versus silica: 1.144 ± 0.05383 versus 2.095 ± 0.1344, $p < 0.0001$). Compared with silica treatments, priming with LPS induced a statistically significant increase in oxygen turnover at 2 h (silica versus LPS/silica: 2.265 ± 0.04950 versus 1.670 ± 0.08485, $p < 0.05$), 6 h (silica versus LPS/silica: 2.850 ± 0.7212

versus 1.905 ± 0.04950, $p < 0.001$) and 24 h (silica versus LPS/silica: 2.095 ± 0.1344 versus 1.310 ± 0.01414, $p < 0.01$) (Fig. 2B).

To assess the production of ROS and oxygen consumption by CII in the forward direction (toward complex V, ATPase enzyme), we performed a SUIT assay, wherein pretreated RAW 264.7 macrophages were incubated with CI inhibitor (rotenone), before stimulation with CII substrate succinate (see *Substrate-uncoupler-inhibitor titration assay.*). The SUIT assay performed on resting cells showed a decrease in O_2 flux after inhibition of CI, followed by a slight recovery of the O_2 consumption and flux resulting from stimulation of CII with succinate. Subsequently, the uncoupler increased the O_2 slope above the baseline, while antimycin A, blocking CIII, cytochrome *c* reductase, and suppressed mitochondrial respiration (Fig. 2C). The sequential treatment of silica exposed RAW 264.7 macrophages with CI inhibitor, and CII substrate confirmed the aforementioned synergistic effect of silica on the enzymatic effect of CII because these cells exhibited a significant time-dependent increase of O_2 consumption, that although identified at 2 h, it peaked at 4–6 h exposure (4 h: 2.221 ± 0.2787, $p < 0.01$; 6 h: 3.824 ± 1.286, $p < 0.0001$), proving a substantial rise in respiration only through CII (Fig. 2D). LPS induced a statistically significant increase of oxygen flux only at 4 h (4.605 ± 1.176; $p < 0.0001$), while priming with LPS before silica exposure induced an enhancement of oxygen turnover only after 24 h (2.514; $p < 0.001$) (Fig. 2D).

The comparison between LPS and silica with or without LPS priming at every time point during the study confirmed that LPS increases the oxygen flux at 4 h (LPS versus silica: 4.605 ± 1.176 versus 2.221 ± 0.2787, $p < 0.001$; LPS versus LPS/silica: 4.605 ± 1.176 versus 1.375 ± 0.2051, $p < 0.0001$) (Fig. 2D). However, silica increased the oxygen flux at 6 h compared with LPS and LPS/silica (LPS versus silica: 0.6788 ± 0.4884 versus 3.824 ± 1.286, $p < 0.0001$; LPS/silica versus silica: 1.320 ± 0.09899 versus 3.824 ± 1.286, $p < 0.001$), while priming with LPS before silica increased the oxygen flux after 24-h coexposure compared with 24-h silica exposure (silica versus LPS/silica: 0.9500 ± 0.1131 versus 2.514, $p < 0.05$) (Fig. 2D).

The integrity of the mitochondrial membrane was also assessed by the addition of the uncoupler. Silica itself did not uncouple the ETC even in the presence of priming, as shown by the increase of O_2 flux after the addition of CCCP (Supplemental Fig. 2). In contrast, LPS markedly damaged the mitochondrial membrane, as shown by the absence of alteration in the O_2 curve after the addition of CCCP (Supplemental Fig. 2).

Subsequently, we then examined the CII-mediated production of H_2O_2 by Amplex Red while subjecting the RAW 264.7 macrophages to the SUIT assay protocol. CI inhibition followed by CII stimulation in resting RAW 264.7 macrophages caused an immediate increment of H_2O_2 generation, similar to the one observed above during the proton leak state. Addition of ADP, inducing CII-linked oxidative phosphorylation (OXPHOS), reduced H_2O_2 production. Furthermore, the uncoupling of the system rebooted the production of H_2O_2 that was ultimately suppressed by CIII inhibition (Fig. 2E). Compared with LPS-treated cells, silica-exposed RAW 264.7 macrophages showed significantly higher production of H_2O_2 6 h after silica exposure, confirming the increased O_2 consumption through CII (Fig. 2F). These findings suggest that silica itself acts within the cells to enhance the activity of mitochondria CII.

Silica inhibits CI activity in part by reducing ECSIT expression

In addition to the high-resolution respirometry, we measured, via the enzymatic assays, the individual activity of CI and CII of silica-exposed RAW 264.7 macrophages. Previously, we have shown that in RAW 264.7 macrophages, silica induces a time-dependent decrease in the expression of the 39-kDa CI subunit; subsequently, CI enzymatic activity was downregulated (8). In agreement with our previous data, we found that silica downregulates CI activity significantly in a time-dependent fashion with lower activity after 6-h exposure, while the nontoxic concentration of LPS (1 ng/ml) did not interfere with the enzyme function of this mitochondrial complex (Fig. 3A). No difference was identified in CII activity between LPS- and/or silica-exposed macrophages (average mean 0.446 ± 0.0325) at baseline (Fig. 3B). Compared with control-treated cells at baseline (baseline 0.4465 ± 0.0325), LPS induced a transient, but not statistically significant, difference in enzymatic activity of CII, observed at 4–18 h after exposure. In contrast, silica significantly enhanced the enzymatic activity of CII as early as 2 h (0.622 ± 0.0492, $p < 0.01$) (Fig. 3B). This statistically significant difference persisted during the 24-h exposure time as follows: 4 h, 0.667 ± 0.110, $p < 0.001$; 6 h, 0.659 ± 0.0692, $p < 0.001$; 18 h, 0.627 ± 0.0609, $p < 0.001$; and 24 h, 0.639 ± 0.101, $p < 0.001$ (Fig. 3B). The comparison between LPS and silica treatment at every time point during the study confirmed that silica induced a statistically significantly greater increase of CII activity at 2 h (LPS versus silica: 0.482 ± 0.0448 versus 0.622 ± 0.0492, $p < 0.05$), 6 h (LPS versus silica: 0.527 ± 0.0371 versus 0.659 ± 0.0692, $p < 0.05$), 18 h (LPS versus silica: 0.502 ± 0.0853 versus 0.627 ± 0.0609, $p < 0.05$), and 24 h (LPS versus silica: 0.422 ± 0.0696 versus 0.639 ± 0.101, $p < 0.001$) (Fig. 3B). The difference between these groups at 4 h was noted but did not achieve statistical significance.

Compared with LPS or silica treatments, priming with LPS before silica exposure induced a statistically significant increase in enzymatic activity of CII only 18 h (LPS/silica versus at baseline: 0.606 ± 0.0188 versus 0.4465 ± 0.0325, $p < 0.01$) and 24 h postexposure (LPS/silica versus at baseline: 0.628 ± 0.0456 versus 0.4465 ± 0.0325, $p < 0.001$) (Fig. 3B). These findings reproduced the results of the respirometry assay, confirming a key role of CII in the mitochondrial response of macrophages to silica.

CI is the largest of the five ETC complexes in the mitochondrial membrane; it consists of 44 core and accessory subunits (20–22). Among the 14 factors involved in this assembly process, *Ecsit* has a key role in the regulation of the stability and activity of the CI and, subsequently, the mitochondrial function (23). To understand the mechanism that drives the decreased enzymatic activity of CI in silica-exposed RAW 264.7 macrophages, we studied by Western blotting the expression of *Ecsit* in the mitochondria of LPS- or silica-exposed cells. In contrast with LPS, which enhances *Ecsit* expression as a function of time (Fig. 3C), mitochondrial protein derived from silica-exposed cells showed a time-dependent decreased abundance of *Ecsit* 6 h after silica exposure (Fig. 3D). This finding was confirmed by direct visualization of the protein using immunofluorescence, wherein cells treated with silica with or without LPS priming exhibit a significantly decreased content of *Ecsit* over time with a peak after 4-h exposure (Fig. 3E, 3F). In contrast, cells treated with LPS did not show a substantial decrease in *Ecsit* protein and demonstrated increased expression of *Ecsit* after 4-h exposure (Fig. 3E, 3F).

The importance of mitochondrial CII activity on macrophage survival to silica

Macrophages differ greatly in their response to silica, and previously we reported that the RAW 264.7 and IC-21 macrophage cell lines, which reproduce the effects of silica on primary mouse macrophages derived from BALB/c and C57BL/6J mice, respectively (18, 24), differ significantly in their viability and cytokine response to silica (8). Thus, although RAW 264.7 macrophages release TNF-α and exhibit a low level of cell cytotoxicity in response to silica, IC-21 macrophages do not release TNF-α and experience universal cell death, even at low concentrations of silica particles (8). Therefore, to better understand the role of mitochondrial CII on macrophage

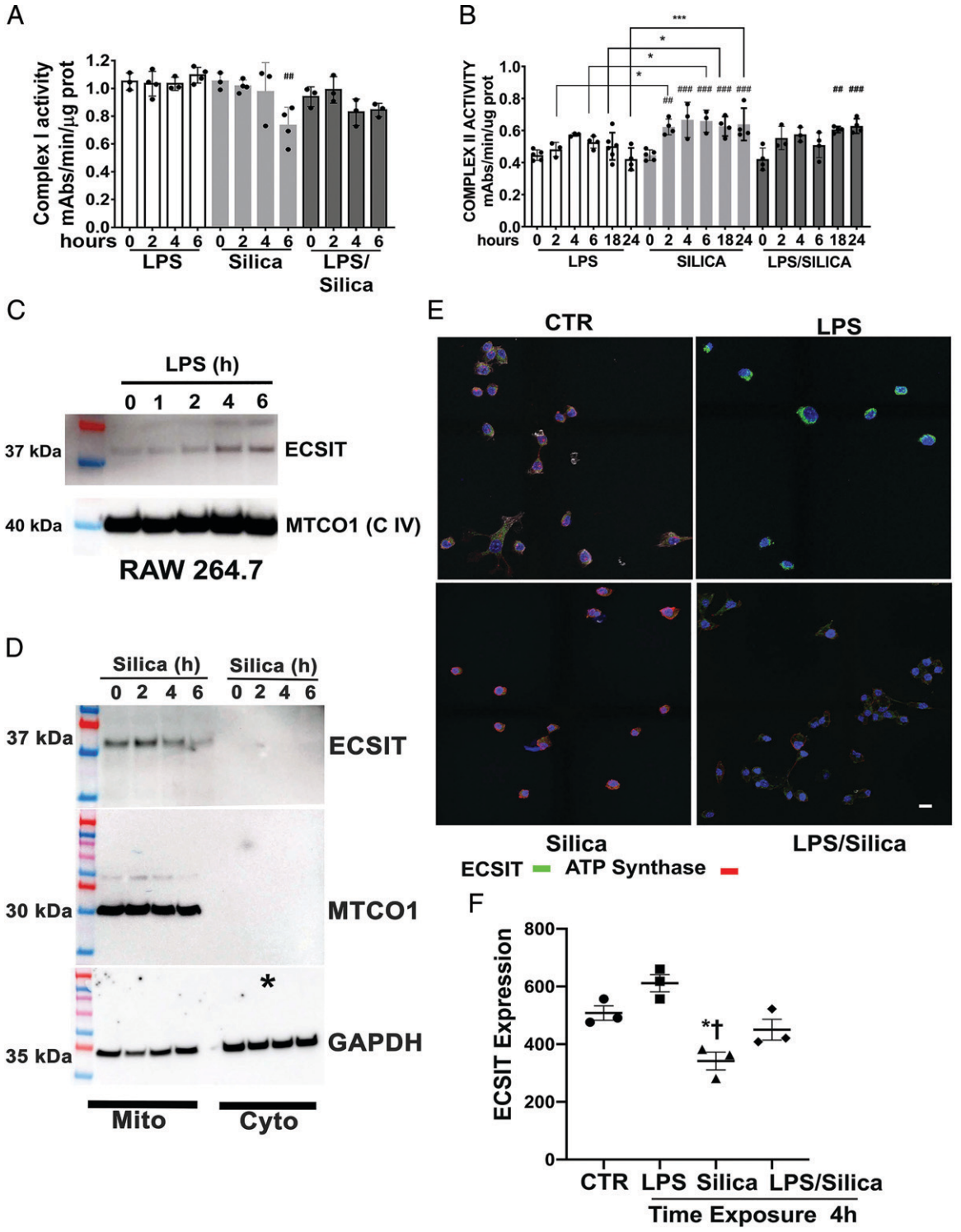

FIGURE 3. Silica inhibits CI activity in part by reducing *Ecsit* expression. RAW 264.7 macrophages were exposed to LPS (1 ng/ml) or silica (50 μg/cm^2) or primed with LPS (1 ng/ml for 24 h) and then exposed to silica (50 μg/cm^2) and examined as a function of time 0–24 h. (**A** and **B**) Mitochondria pellets were isolated from RAW 264.7 macrophages, and complex I and complex II enzymatic activity were analyzed spectrophotometrically and measured as mAbs/min/μg proteins (see *CI assay* and *CII assay.*). $n = 4$. (**C** and **D**) Mitochondria were isolated from RAW 264.7 macrophages exposed to LPS (C) or silica (D) for the indicated times, and *Ecsit* (37-kDa subunit) abundance was determined by Western blot while using complex IV subunit MTCO1 as markers for mitochondria and GAPDH expression as a loading control. (**E**) Confocal microscopy of RAW 264.7 macrophages stimulated for 4 h with LPS (1 ng/ml) or silica (50 μg/cm^2) in the presence or absence of LPS priming. Mitochondria are visualized by staining with ATPase (red), DNA into the nuclei of cells with Hoechst (blue), followed by the analysis of *Ecsit* (green). Scale bar: 10 μm. (**F**) Graph illustrating the abundance of ESCIT in LPS- or silica-exposed RAW 264.7 macrophages. Data are expressed as the mean ± SEM and are representative of three different experiments. *$p < 0.05$, ***$p < 0.001$, LPS versus silica; $^{\#\#}p < 0.01$, $^{\#\#\#}p < 0.001$ versus baseline. CTR, control.

survival, we compared the effect of silica particles on the enzymatic activity of CII on RAW 264.7 and IC-21 macrophages.

Our studies on cell viability demonstrated that although silica induced significant cell cytotoxicity and LDH release in IC-21 macrophages, LPS does not significantly impact these parameters 6–24 h after exposure (Fig. 4A, 4B). Importantly, the addition of silica to IC-21 macrophages primed with a nontoxic concentration of LPS resulted in a synergistic effect that reduced the cell survival to 5% at 24 h postexposure (Fig. 4A, 4B).

Under these experimental conditions, LPS-stimulated IC-21 macrophages enhanced the release of lactate to a greater extent than IC-21 macrophages exposed to silica (Fig. 4C). In addition, in contrast with the data described earlier for RAW 264.7 macrophages, stimulation of CII with succinate, in the presence or absence of rotenone inhibition of CI, does not affect the oxygen flux, nor the mitochondrial ROS production in LPS-treated IC-21 macrophages (Fig. 4D–F). In contrast with LPS, silica particles induced significant increases in the oxygen flux and mitochondrial ROS production in IC-21 macrophages (Fig. 4D–F), suggesting that the enzymatic activity of CI was not affected by silica exposure on IC-21 macrophages (Fig. 4G). Conversely, CII activity was significantly inhibited in IC-21 macrophages by silica alone as early as 2 h postexposure, even after LPS priming (Fig. 4H).

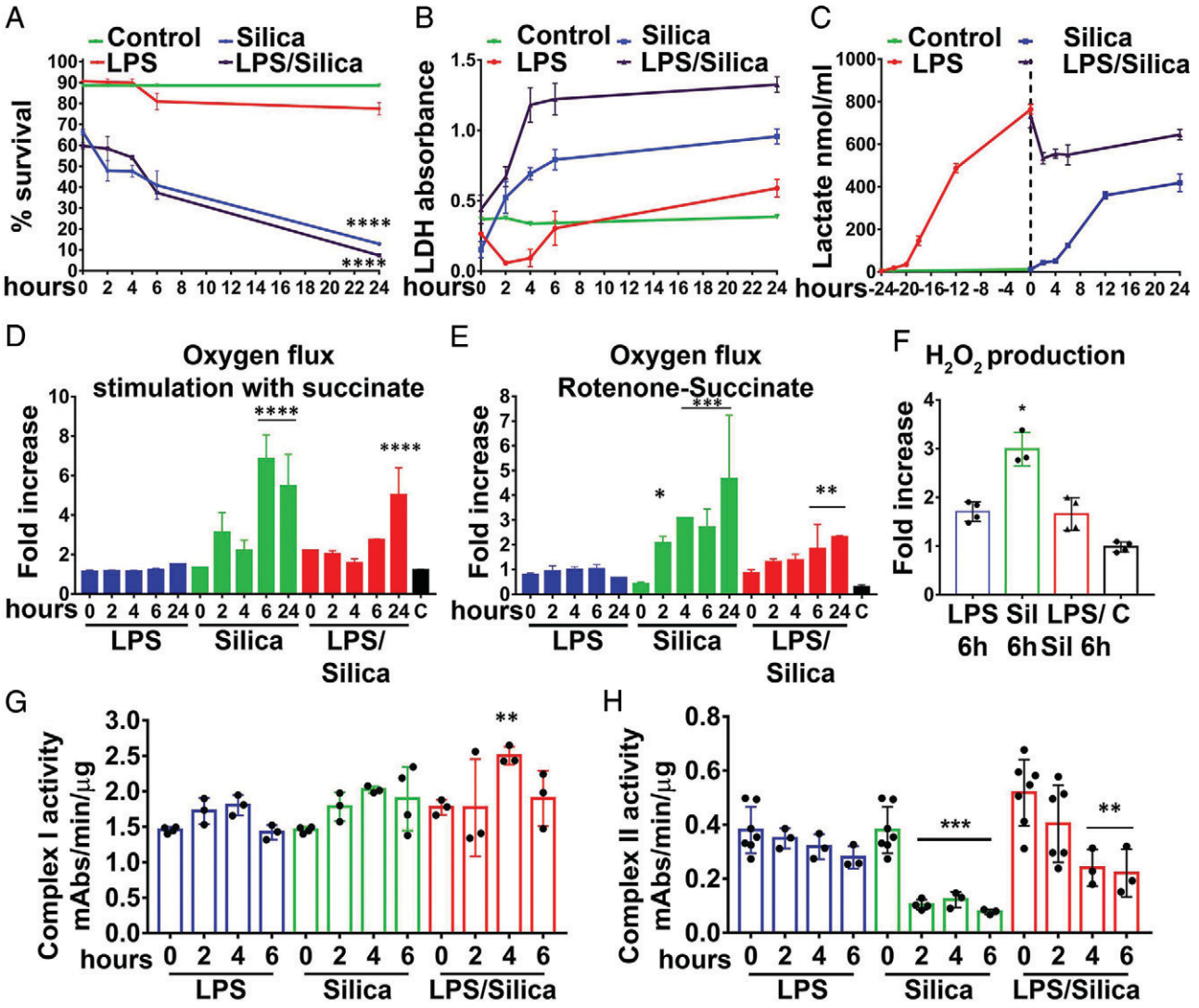

FIGURE 4. The importance of mitochondrial complex II activity on macrophage survival in response to silica. IC-21 macrophages were exposed to LPS (1 ng/ml) or silica (50 µg/cm^2), or primed with LPS (1 ng/ml for 24 h) and then exposed to silica (50 µg/cm^2) for up to 24 h. (**A**) Annexin V and PI were used to analyze cell survival by flow cytometry: graph summarizing the survival of cells treated as above. (**B** and **C**) The supernatants of cells were examined for released LDH and lactate. (**D**–**F**) Respirometric analysis: IC-21 macrophages (2.5×10^6/chamber) were allowed to equilibrate in the chamber for ~10 min before measuring oxygen flow. Default respirometric settings of block temperature 37°C, stir bar speed 400 rpm, and data recording every 2 s were used. Oxygen turnover by treated IC-21 macrophages was followed after addition of (D) succinate 10 mM or (E) rotenone (f.c., 0.5 µM), succinate (f.c., 10 mM), ADP (f.c., 2.5 mM), CCCP (f.c., 0.05 µM), and antimycin A (f.c., 2.5 µM). After the addition of each compound, cells were allowed to come to equilibrium. Variations in oxygen flux for each condition were measured as a ratio between the value of the O_2 slope at the equilibrium after treatment with succinate (with or without previous treatment with rotenone) and the value of O_2 slope at the baseline. (D) Fold increase of oxygen flux after stimulation with succinate. (E) Fold increase of oxygen flux after the inhibition of CI with rotenone and stimulation of CII with succinate. (F) The production of H_2O_2 has been assessed following the concentration of the fluorescent Amplex Red assay product resorufin while performing a SUIT assay protocol. Variations in H_2O_2 for each condition were measured as the ratio between the value of the slope at the equilibrium after the inhibition of CI with rotenone and the stimulation of CII with succinate and the value of the slope at baseline. $n = 3$. (**G** and **H**) Mitochondria pellets were isolated from IC-21 macrophages, and CI and CII enzymatic activity were measured spectrophotometrically and measured as mAbs/min/µg proteins. $n = 3$; $^*p < 0.05$, $^{**}p < 0.01$, $^{***}p < 0.001$, $^{****}p < 0.0001$ versus control.

Silica and LPS exert similar effects on glucose uptake and glycolysis but differ on the effects on the TAC in macrophages

LPS-stimulated macrophages exhibit immunometabolic regulation, leading to perturbations of glycolysis and the TAC that contribute to cytokine specification (11, 25–29). To investigate the effects of silica on glucose metabolism and the TAC activity of RAW 264.7 macrophages, we fed cells with $[^{13}C]_6$-glucose and conducted a stable isotope tracer analysis using high-resolution mass spectrometry to discern subtle shifts in energy substrate metabolism, through the detection and quantification of metabolite isotopologues from control, noncytotoxic dose of silica-exposed (50 μg/cm^2), or LPS-exposed (10 ng/ml) macrophages (Supplemental Fig. 3). Our LC-HRMS analysis revealed that when compared with control cells, both LPS and silica induce an increase in the uptake and phosphorylation of glucose, as illustrated by intracellular enrichment in glucose-6-phosphate and glyceraldehyde-3-phosphate (Fig. 5A–C). Isotopologues analysis shows that compared with control cells, both silica- and LPS-exposed RAW 264.7 macrophages exhibit greater, but comparable, enrichment in intracellular levels of pyruvate and lactate (Fig. 5D–F). However, LPS-treated RAW 264.7 macrophages demonstrate a greater ratio (0.38) of conversion of pyruvate into lactate when compared with control (0.29) or silica-exposed (0.33) macrophages, leading to a greater intracellular (Figs. 1 and 5) and extracellular (Supplemental Fig. 4) enrichment in lactate.

Compared with control or silica-treated RAW 264.7 macrophages, LPS induces an increase in the intracellular relative amount of the TAC intermediates glutamine, succinate, fumarate, malate, and itaconate, while maintaining the levels of citrate, α-ketoglutarate, and glutamate (Fig. 6A–H). In addition, LPS-stimulated cells show enrichment of glutamine, proline, and arginine, derived from these intermediates (Fig. 6G, 6I, 6J). In contrast with control or LPS-exposed macrophages, intracellular levels of citrate are not detectable in silica-exposed macrophages (Fig. 6A), and these silica-exposed macrophages exhibit significant reduction, compared with control or LPS-stimulated cells, in the intracellular levels of α-ketoglutarate, itaconate, succinate, fumarate, malate, glutamine, and glutamate (Fig. 6A–H).

Our data show that both LPS and silica influence the enzymatic activity of SDH, an enzyme that plays a fundamental role in both glycolysis and ETC (Figs. 2D and 3B). Glutamine-dependent anaplerosis is the principal source of succinate, although the "γ-aminobutyric acid shunt" pathway also has a role in LPS-stimulated macrophages. Therefore, we measured the conversion of glutamate into succinate. LPS-treated macrophages show increased rates (0.59) of glutamate conversion to succinate (Fig. 5G). This conversion was not significantly altered by silica, and isotopologues analysis showed that although the baseline glutamate enrichment was comparable among control, LPS-, or silica-treated cells (M+0 to M+4), a higher enrichment of succinate was detected at M+2 only in LPS-exposed macrophages (Fig. 6K, 6L).

LPS, but not silica exposure, induces stabilization of HIF-1α, activation of NLRP3 inflammasome, and release of IL-1β

As we described in the *Introduction*, LPS-stimulated macrophages exhibit altered intracellular metabolic changes that specify immune effector mechanisms, such as cytokine secretion. To determine whether these changes also take place in silica-exposed macrophages, we correlated the metabolic changes observed in RAW 264.7 macrophages in response to silica with the production of IL-1β, TNF-α, and INF-β, three cytokines that have been implicated in the pathogenesis of silicosis (30). In bone marrow-derived macrophages (BMDMs), LPS enhances succinate levels, leading to succinate-mediated stabilization of HIF-1α, activation of NLRP3 inflammasome, and IL-1β production (11, 13, 31, 32). In this work, we find that in contrast with LPS, silica reduced the intracellular levels of succinate below the baseline levels observed in unstimulated RAW 264.7 macrophages (Fig. 6D). To assess the correlation between the SDH activity, the level of succinate, and expression of HIF-1α, we stimulated RAW 264.7 macrophages with silica for 6 h, with or without priming with LPS (1 ng/ml for 24 h). Giving the well-known sensitivity of HIF-1α gene to oxygen tension, we documented the ability of silica or LPS to stabilize HIF-1α expression under either normoxic (O_2 = 20%) or hypoxic (O_2 less than 5%) conditions. Silica, as well as LPS, promoted the time-related stabilization of HIF-1α protein under normoxic conditions, as demonstrated via immunoblotting (Fig. 7A, upper panel) and confirmed by immunofluorescence and quantitative analysis of nuclear localization (Fig. 7B, 7C).

However, these changes on HIF-1α protein expression, which were accentuated by hypoxia, were associated with activation of the NLRP3 inflammasome, documented by the cleavage of pro-caspase-1 into low m.w. (p10) mature caspase-1 and the fragmentation and

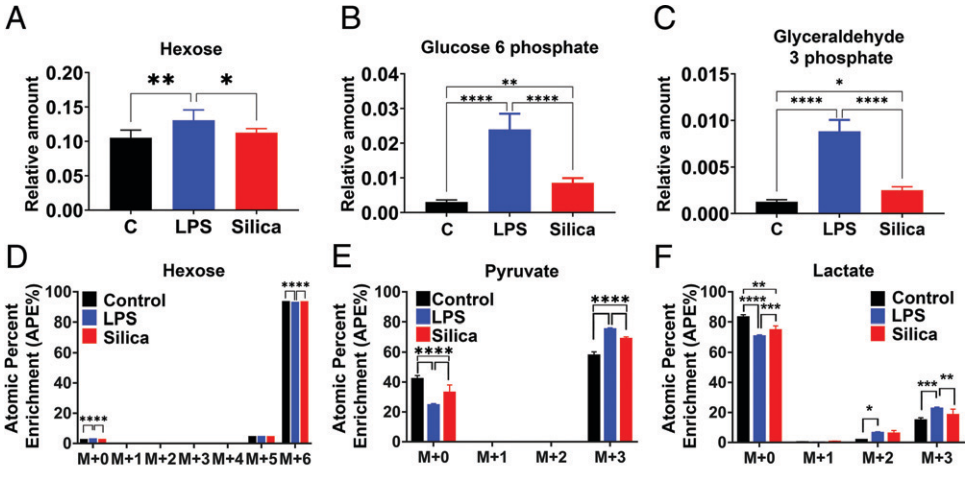

G

	CONVERSION RATIO		
	CONTROL	LPS	SILICA
PYRUVATE/HEXOSE	0.594	0.775	0.687
LACTATE/PYRUVATE	0.291	0.388	0.331
LACTATE/HEXOSE	0.173	0.301	0.227
SUCCINATE/GLUTAMATE	ND	0.594	ND

FIGURE 5. Silica and LPS exert similar effects on glucose uptake and glycolysis in macrophages. RAW 264.7 macrophages were treated with LPS (10 ng/ml) or silica (50 μg/cm^2) or left untreated for 6 h. (**A**–**C**) Intracellular relative amount of hexose uptake and glycolytic metabolites glucose-6-phosphate and glyceraldehyde-3-phosphate. (**D**–**F**) $[^{13}C]_6$ uptake and intracellular pyruvate and lactate enrichment were determined by LC-HRMS. Atomic percent enrichment was calculated using the MIMOSA method. Data are the mean ± SEM of six samples, $n = 6$; $^*p < 0.05$, $^{**}p < 0.01$, $^{***}p < 0.001$, $^{****}p < 0.0001$, control versus LPS versus silica. (**G**) Table representing the conversion ratio of selected metabolites calculated dividing the total enrichment (sum of absolute number M+1 to M+6) of the product by the total enrichment of the reactant.

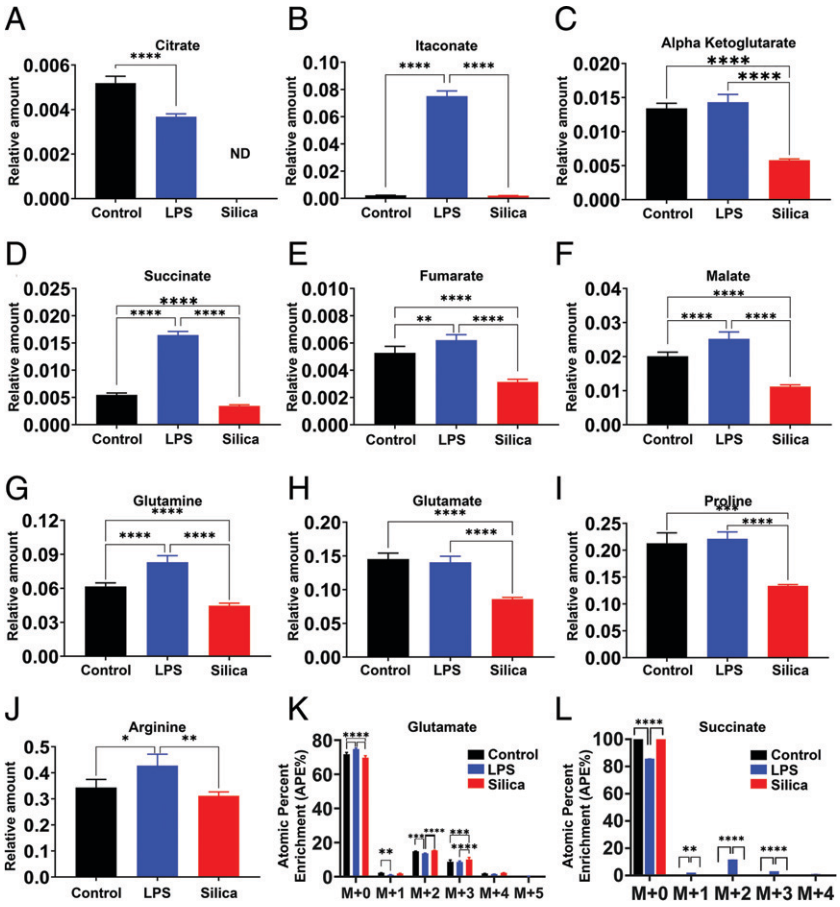

FIGURE 6. Silica and LPS affect TAC in a differential manner. RAW 264.7 macrophages were treated with LPS (10 ng/ml) or silica (50 μg/cm^2) or left untreated for 6 h. (**A–L**) Intracellular relative amount of TAC (A–F) metabolites and (G–J) amino acids. (K and L) Changes in succinate and glutamate atomic percent enrichment at steady state determined by LC-HRMS. Atomic percent enrichment was calculated using the MIMOSA method. Data are the mean ± SEM of six samples; $n = 6$; *$p < 0.05$, **$p < 0.01$, ***$p < 0.001$, ****$p < 0.0001$, control versus LPS versus silica.

release of IL-1β only in LPS-stimulated RAW 264.7 macrophages (Fig. 7A, middle panel). Yet, silica-stimulated RAW 264.7 macrophages demonstrated enhanced IL-1β mRNA and release of IL-1β peptide in culture in the absence of pro-caspase-1 activation (Fig. 7D, 7E), suggesting that silica-induced IL-1β production could take place independent of succinate-associated HIF-1α-mediated NLRP3 inflammasome activation.

Malonylation of GAPDH correlates with TNF-α production in LPS, but not in silica-exposed macrophages

The citrate-derived metabolite malonyl-CoA induces the malonylation of multiple proteins, including GAPDH, specifically on lysine 213. In resting cells, GAPDH sequesters the TNF-α mRNA, blocking its translation. On LPS stimulation, GAPDH undergoes malonylation, a reaction that facilitates the release of TNF-α mRNA for transcription and subsequent secretion (33). In our study, we find that LPS, as well as silica, stimulated macrophages to release TNF-α in a dose-dependent manner (Fig. 8A). Compared with nonstimulated RAW 264.7 macrophages, silica, as well as LPS, enhanced GAPDH and TNF-α mRNA expression (Fig. 8B). However, immunoprecipitation of GAPDH from protein lysates obtained from silica or LPS-stimulated RAW 264.7 macrophages identified GAPDH malonylation in a manner that proceeded TNF-α release, exclusively in LPS-exposed macrophages (Fig. 8C).

Decreased itaconate levels correlate with decreased IFN-β in silica-exposed macrophages

The anti-inflammatory features of the TAC metabolite itaconate have been described in LPS-treated macrophages. Endogenous itaconate regulates succinate levels and limits IL-1β production in LPS-activated macrophages (34, 35). Our data show that LPS-activated RAW 264.7 macrophages increase the intracellular amount of itaconate, while silica-activated macrophages reduce the concentrations of this TAC intermediate below control levels (Fig. 8F). Thus, LPS (10 ng/ml) significantly stimulates the transcription of IFN-β in macrophages during 24-h exposure, whereas silica (50 μg/cm^2) significantly reduces the transcription and release of this mediator during the first 12 h, and increased levels for IFN- β mRNA were observed only at 24 h postexposure (Fig. 8D). However, the increased levels in IFN-β mRNA 24 h after silica exposure were significantly ($p < 0.05$) lower than those observed in LPS-treated cells at the same time (Fig. 8D). Release of IFN-β by RAW 264.7 macrophages parallels the increase in mRNA, with statistically significant levels of the cytokine detected by ELISA 6–24 h after LPS, but not in silica-stimulated macrophages. LPS priming of macrophages before silica exposure reconstitutes IFN-β mRNA expression and the ability of RAW 264.7 macrophages to secrete this cytokine (Fig. 8D, 8E). The addition of silica to LPS-primed RAW 264.7 macrophages restores the ability of RAW 264.7 macrophages to release IFN-β in a synergistic manner (Fig. 8E).

Discussion

The main finding of this work is that in contrast with the prevalent view, respirable, sterile, crystalline silica alone is capable of inducing an innate immune response without requiring previous macrophage activation by LPS. This silica-induced activation of macrophages is different from the LPS-induced activation, because they affect differently the CII of ETC, which plays a crucial role in macrophage survival and silica-induced inflammatory response.

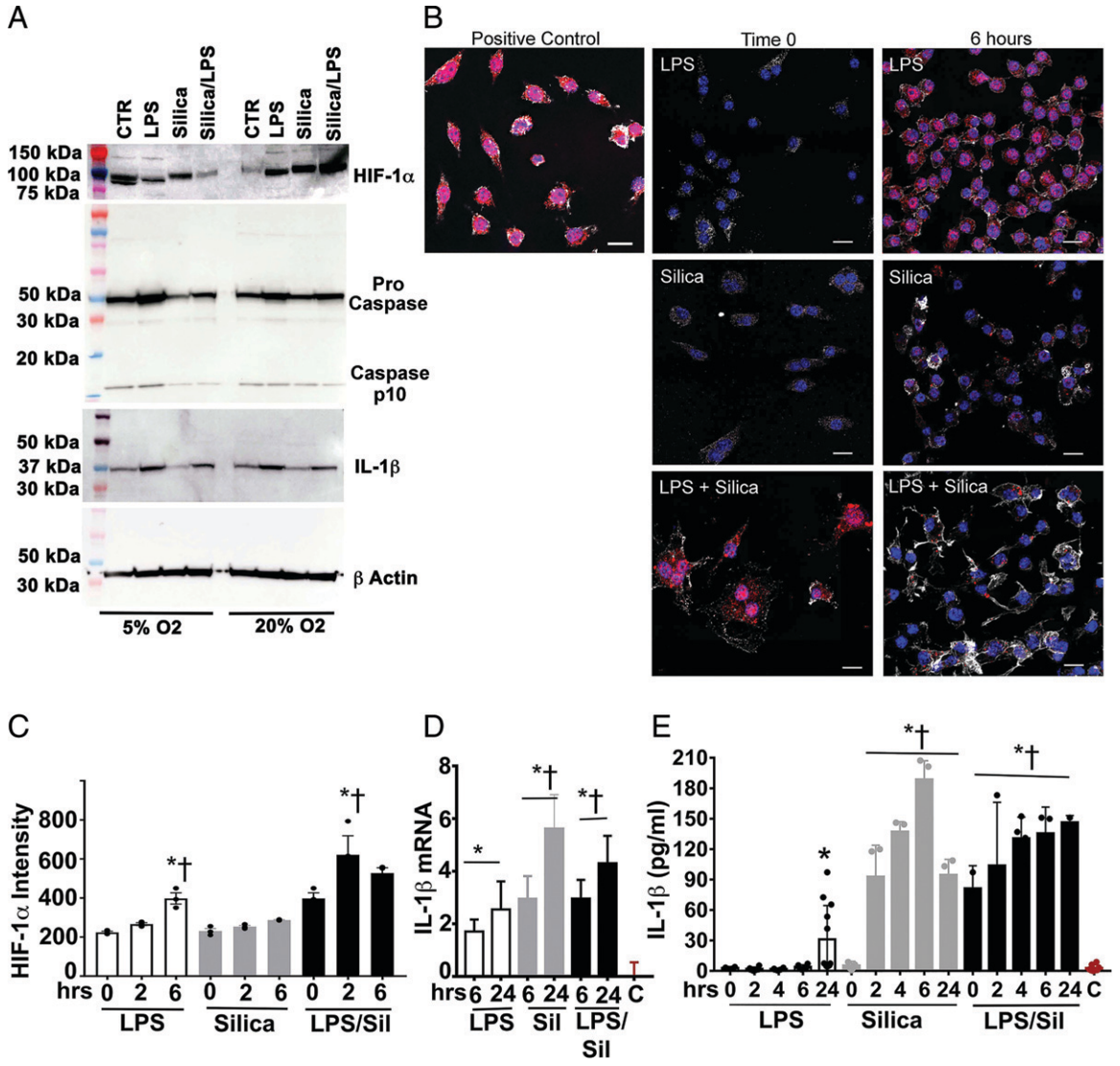

FIGURE 7. LPS, but not silica, exposure induces stabilization of HIF-1α, activation of NLRP3 inflammasome, and release of IL-1β. RAW 264.7 macrophages were stimulated with LPS (1 ng/ml) for 24 h, silica (50 μg/cm^2) for 6 h, with or without priming, or left untreated. Cells were incubated in normoxia (20% oxygen) or hypoxia (<5% oxygen). (**A**) Proteins were isolated from RAW 264.7 macrophages exposed as described, and HIF-1α (110-kDa subunit) abundance, pro-caspase-1, caspase-1 (10 kDa), and IL-1β (37 kDa) were determined by Western blot while using β-actin expression as a loading control. (**B**) Confocal microscopy of RAW 264.7 macrophages stimulated for 6 h with LPS (1 ng/ml) or silica (50 μg/cm^2) in the presence or absence of priming. DNA into the nuclei of cells is visualized with Hoechst; cytoskeleton filaments were visualized with actin Ab (white), followed by the analysis of HIF-1α (red). Scale bars: 10 μm. (**C**) Graph illustrating the abundance of HIF-1α in LPS- or silica-exposed RAW 264.7 macrophages. Data are expressed as the mean ± SEM and are representative of three different experiments. (**D**) IL-1β mRNA expression levels quantified by RT-PCR in RAW 264.7 macrophages exposed to LPS or silica or LPS and silica for the indicated time (0, 6, or 24 h). (**E**) ELISA of IL-1β release in the supernatant by RAW 264.7 macrophages stimulated as indicated. Data are the mean ± SEM of six samples, $n = 6$. *$p < 0.05$, versus control; †$p < 0.0001$ versus silica treated.

In contrast with LPS, very little data are available regarding the metabolic reprogramming of macrophages in silica-induced inflammation and subsequent development of silicosis. The purpose of our study is to elucidate critical aspects of silica-induced fibrotic inflammation, comparing the metabolic effect of low-dose LPS with silica with or without priming with LPS.

LPS-activated macrophages switch their metabolism from OXPHOS to aerobic glycolysis, the "Warburg effect" (36), which consists of increased uptake of glucose, glycolysis rate, and subsequent secretion of lactate, in conjunction with a reduced level of OXPHOS via the TAC (11). In our study, we found that nontoxic concentrations of LPS, as well as silica, induce increased uptake of hexoses, increased the relative amount of intracellular glycolytic metabolites, and augmented the relative amount of both intracellular and extracellular lactate. Moreover, priming of macrophages with LPS before silica exposure enhanced cytotoxicity and the observed effect of LPS alone.

In a recent study, Garaude et al. (12) reported that after phagocytosis of live bacteria, BMDMs showed alterations in the assembly of the ETC supercomplexes, consisting of reduced CI activity and enhanced CII abundance and activity. These findings were not observed when BMDMs were stimulated with LPS (12). Consistent with this work, our study demonstrates that shortly after macrophages engulf silica particles, they form phagosomes and recruit mitochondria to these structures (Supplemental Fig. 1). Concomitant to these ultrastructural findings, silica-exposed macrophages remodel the activity of ETC and increase mitochondrial oxygen flux through CII, 2 h postexposure, even after the inhibition of CI with rotenone (Fig. 2). In contrast with silica, LPS induces only a transitory enhancement on mitochondrial respiration in the absence of

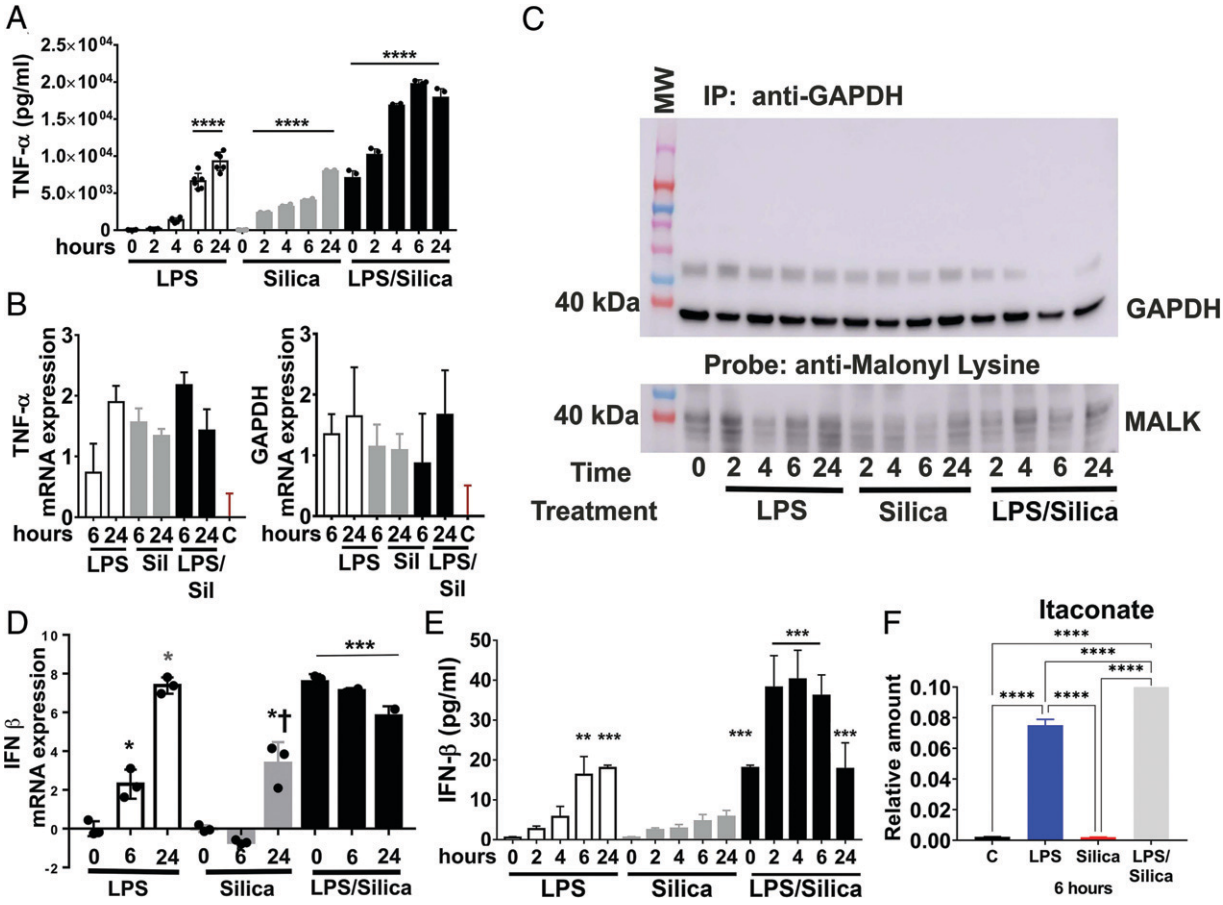

FIGURE 8. Malonylation of GAPDH correlates with TNF-α production in LPS-treated macrophages, while decreased itaconate levels correlate with decreased IFN-β in silica-exposed macrophages. (**A–C**) RAW 264.7 macrophages were stimulated with LPS (1 ng/ml) or silica (50 μg/cm^2) with or without priming and examined at time points up to 24 h. (A) Cell supernatants were examined for TNF-α secretion using ELISA. (B) TNF-α and GAPDH mRNA expression levels quantified by RT-PCR. (C) Immunoprecipitated GAPDH from RAW 264.7 macrophages treated as indicated. Samples probed with an anti-malonyl lysine (anti-MALK) Ab (lower panel). GAPDH expression in the immunoprecipitated (upper panel) samples was also examined. (**D** and **E**) RAW 264.7 macrophages were treated with LPS (10 ng/ml) or silica (50 μg/cm^2) with or without priming. (D) IFN-β mRNA expression levels quantified by RT-PCR in RAW 264.7 macrophages treated as described for the indicated time. (E) ELISA of IFN-β released in supernatant shows that cells exposed to silica or LPS secrete the same amount of cytokine, but silica inhibits the release in primed cells. (**F**) The intracellular relative amount of itaconate at a steady state is determined by LC-HRMS. Atomic percent enrichment was calculated using the MIMOSA method. Data are the mean ± SEM of six samples, $n = 6$. *$p < 0.05$, **$p < 0.01$, ***$p < 0.001$, ****$p < 0.0001$.

mitochondrial CI inhibition by rotenone (Fig. 2). The measurement of mitochondrial ROS production also revealed that silica engulfment is more efficient than LPS in the induction of mitochondrial H_2O_2 release from the activated macrophages. Priming of macrophages with LPS before silica treatment did not enhance the effect of silica on CII or the production of mitochondrial ROS (Fig. 2). The analysis of the kinetic enzymatic activity of CI and CII also confirmed that although LPS did not alter CI activity, it only slightly enhanced CII activity, 4–6 h postexposure, in contrast with silica, which significantly decreased CI activity while simultaneously enhancing CII activity (Fig. 3).

The most commonly observed CI dysfunctions are explained by alterations in CI subunits critical for its assembly. *Ecsit* is a CI subunit that plays a critical role in both the CI assembly stability and the metabolic activity of the complex in macrophages (21, 23, 37). This confers an essential role for *Ecsit* in the antibacterial response of macrophages because of its involvement in the recruitment of mitochondria around the site of intracellular bacteria (38) and its regulation of mitochondrial ROS production from the ETC (23). In our study, the downregulation of *Ecsit* occurs in silica-exposed, but not in LPS-exposed, macrophages in a time-dependent manner, supporting the notion that this protein plays an essential role in the modulation of CI activity in response to silica.

Using IC-21 macrophages that we previously demonstrated generate a greater amount of mitochondrial ROS, experience higher levels of cell death, and secrete lower amounts of TNF-α than RAW 264.7 macrophages in response to silica (8), we further show evidence supporting the notion that in the absence of a functional CI, the enhanced activity of mitochondrial CII is fundamental to preserve mitochondrial respiration and the survival of macrophages in response to silica. Thus, in IC-21 macrophages, CI activity is preserved (Fig. 4), and in contrast with RAW 264.7 macrophages, silica exposure rapidly diminishes, as early as 2 h, the enzymatic activity of mitochondrial CII (Fig. 4), and oxygen flux proceeds via mitochondrial CI activity, leading to greater amount of mitochondrial ROS generation that we previously show contributes to cardiolipin oxidation and cell death (8).

Our data also support the concept that although both LPS and silica stimulate aerobic glycolysis, they affect the TAC differently. An important difference observed between LPS- and silica-stimulated macrophages in the activity of the TAC is the accumulation of succinate, which acts as a potent proinflammatory signal (11, 13). LPS-

induced increases in succinate can be explained by several mechanisms, including the inhibition of SDH, as well as replenishment of succinate from glutamine through the anaplerosis of α-ketoglutarate or through the γ-aminobutyric acid shunt (11). In contrast, silica induces an overall intracellular depletion of TAC metabolites and amino acids, including succinate, α-ketoglutarate, fumarate, glutamine, and glutamate (Figs. 5 and 6). These data suggest that in contrast with LPS, silica enhances the enzymatic activity of mitochondrial CII, demonstrated here as enhanced CII-mediated mitochondrial respiratory, in the absence of a functional CI (Fig. 2). This CII activity enhances TAC dynamics with consumption, rather than accumulation, of succinate. Similarly, our data show that silica does not enhance the conversion of glutamate into succinate observed in LPS-exposed macrophages (Fig. 5).

Activated macrophages exhibit altered immunometabolism: intracellular metabolic changes governing immune effector mechanisms, such as cytokine secretion. Similar to LPS, silica-treated RAW 264.7 macrophages release TNF-α and IL-1β in a dose-dependent manner (Figs. 7 and 8). However, studies in LPS-stimulated macrophages show that these metabolic changes contribute to the production of TNF-α and IL-1β by different mechanisms, leading to cytokine specification (11). Thus, inhibiting glycolysis or blocking SDH in LPS-stimulated macrophages inhibits IL-1β, but not TNF-α, production (11). In macrophages, succinate is an inflammatory signal that contributes to the activation of NLRP3 inflammasome (13, 32). These effects, described in LPS-stimulated macrophages, are mediated via the stabilization of HIF-1α that subsequently induces transcription of HIF-1α target genes, such as IL-1β (11, 13, 31, 32). In this work, we find that silica-stimulated RAW 264.7 macrophages demonstrate stabilization of HIF-1α and enhanced transcription and release of IL-1β (Fig. 7). However, in contrast with LPS, these silica-induced changes occur in the presence of decreased levels of intracellular succinate (Fig. 6) and are unrelated to NLRP3 inflammasome activation because these RAW 264.7 macrophages do not show caspase-1 activation in response to silica particles alone (Fig. 7). Importantly, previous reports demonstrating the ability of silica to activate the NLRP3 inflammasome were conducted in LPS-primed macrophages (7, 30, 39).

The role of TNF-α in the pathogenesis of silicosis is well recognized (40). However, the mechanisms specifying TNF-α production by silica-exposed macrophages are not entirely understood. Recent information shows that macrophage secretion of TNF-α and IFNs in response to LPS is mediated, in part, via malonylation of GAPDH (33, 41, 42). White et al. (43) identified a role for GAPDH as a noncanonical RNA-binding protein. In resting macrophages, GAPDH binds to and suppresses the translation of inflammatory mRNAs, including IFN-β and TNF-α (43). GAPDH binds NAD^+ to retain mRNA silence. LPS-induced malonylation of GAPDH requires the separation of NAD^+ from the enzymatic domain to facilitate protein malonylation on lysine 213 (33). However, in this work, we documented lysine 213 malonylation only on protein precipitates from LPS-exposed RAW 264.7 macrophages, in a manner that precedes the transcription and release of TNF-α (Fig. 8). These data agree with previous observations linking the silica-induced TNF-α generation to NADPH- and mitochondrial ROS-mediated NF-κB activation and TNF-α mRNA transcription (38, 44, 45).

The anti-inflammatory properties of itaconate, a TAC metabolite generated through the decarboxylation of *cis*-aconitate, a product of citrate, have also been described in LPS-activated macrophages (46). LPS-induced accumulation of itaconate, mainly because of the isocitrate dehydrogenase impairment, can regulate the SDH activity, thereby decreasing the inflammatory response, and also regulate the IFN-β secretion (35, 47). In this study, we observed that, although the intracellular level of itaconate is significantly augmented in LPS-activated macrophages, the same does not occur after silica engulfment; consequently, this directly correlates with the transcription and release of IFN-β in response to either LPS or silica (Fig. 8).

Previous in vivo studies demonstrated that macrophage ontogeny plays a crucial role in their immunometabolic response (15). Specifically, increased glycolysis-driven and decreased TAC-driven metabolism on bacterial activation is observed in macrophages recruited to the lung, while stable or minimal alteration of glycolysis and TAC enzymes and increased fatty acid oxidation are observed in resident alveolar macrophages (14–16). A limitation to the current studies is that the data were procured with the use of macrophage cell lines. RAW 264.7 and IC-21 cells, which are derived from resident peritoneal macrophages, demonstrate baseline rates of glycolysis, phospholipid content, and fatty acid oxidation that are representative of human monocyte-derived macrophages (8), as well as those observed in primary alveolar macrophages from their corresponding mouse strains, C57BL/6 or BALB/c, respectively (8, 48). Therefore, further in vivo studies are required to fully comprehend the difference in the immunometabolic response to inhaled crystalline silica of alveolar and interstitial macrophages, as well as monocyte recruited from the peripheral circulation into the lung in response to silica exposure.

In summary, this work indicates that on internalization into phagolysosomes, respirable crystalline silica drives a metabolic adaptation of macrophages consisting of increased uptake of glucose, increased glycolysis, accompanied by an increased lactate secretion, at the expense of the OXPHOS, which becomes sustained only by increased CII activity, while CI activity is reduced. Given the role of CII as a component of both the TAC and the ETC, its activity becomes a key regulator of macrophages' survival. Silica also modulates the TAC, where not only the succinate level is measured below baseline but also the total intracellular level of all key TAC intermediates, and amino acids examined are decreased probably as a result of high demand and consumption. In contrast with LPS, these silica-induced metabolic adaptations do not correlate with IL-1β and TNF-α production but with the suppressed release of IFN-β. Further studies are needed to validate this concept and to better understand the mechanisms that induce the release of inflammatory cytokines after the phagocytosis of silica into macrophages.

Disclosures

The authors have no financial conflicts of interest.

References

1. Gottesfeld, P., M. Reid, and E. Goosby. 2018. Preventing tuberculosis among high-risk workers. *Lancet Glob. Health* 6: e1274–e1275.
2. Leung, C. C., I. T. S. Yu, and W. Chen. 2012. Silicosis. *Lancet* 379: 2008–2018.
3. Anderson, S. E., H. Shane, C. Long, A. Marrocco, E. Lukomska, J. R. Roberts, N. Marshall, and J. S. Fedan. 2020. Biological effects of inhaled hydraulic fracturing sand dust. VIII. Immunotoxicity. *Toxicol. Appl. Pharmacol.* 408: 115256.
4. Di Giuseppe, M., F. Gambelli, G. W. Hoyle, G. Lungarella, S. M. Studer, T. Richards, S. Yousem, K. McCurry, J. Dauber, N. Kaminski, et al. 2009. Systemic inhibition of NF-kappaB activation protects from silicosis. *PLoS One* 4: e5689.
5. World Health Organization. 2007. Elimination of silicosis. *GOHNET newsletter*, p. 1–20. Available at: https://www.who.int/occupational_health/publications/newsletter/gohnet12e.pdf?ua=1.
6. Investigative Team. 2020. Biological effects of inhaled hydraulic fracturing sand dust. IX. Summary and significance. *Toxicol. Appl. Pharmacol.* 409: 115330.
7. Cassel, S. L., S. C. Eisenbarth, S. S. Iyer, J. J. Sadler, O. R. Colegio, L. A. Tephly, A. B. Carter, P. B. Rothman, R. A. Flavell, and F. S. Sutterwala. 2008. The Nalp3 inflammasome is essential for the development of silicosis. *Proc. Natl. Acad. Sci. USA* 105: 9035–9040.
8. Fazzi, F., J. Njah, M. Di Giuseppe, D. E. Winnica, K. Go, E. Sala, C. M. St Croix, S. C. Watkins, V. A. Tyurin, D. G. Phinney, et al. 2014. TNFR1/phox interaction and TNFR1 mitochondrial translocation Thwart silica-induced pulmonary fibrosis. *J. Immunol.* 192: 3837–3846.

9. Tschopp, J., and K. Schroder. 2010. NLRP3 inflammasome activation: The convergence of multiple signalling pathways on ROS production? *Nat. Rev. Immunol.* 10: 210–215.
10. Mischler, S. E., E. G. Cauda, M. Di Giuseppe, L. J. McWilliams, C. St Croix, M. Sun, J. Franks, and L. A. Ortiz. 2016. Differential activation of RAW 264.7 macrophages by size-segregated crystalline silica. *J. Occup. Med. Toxicol.* 11: 57.
11. Tannahill, G. M., A. M. Curtis, J. Adamik, E. M. Palsson-McDermott, A. F. McGettrick, G. Goel, C. Frezza, N. J. Bernard, B. Kelly, N. H. Foley, et al. 2013. Succinate is an inflammatory signal that induces IL-1β through HIF-1α. *Nature* 496: 238–242.
12. Garaude, J., R. Acín-Pérez, S. Martínez-Cano, M. Enamorado, M. Ugolini, E. Nistal-Villán, S. Hervás-Stubbs, P. Pelegrín, L. E. Sander, J. A. Enríquez, and D. Sancho. 2016. Mitochondrial respiratory-chain adaptations in macrophages contribute to antibacterial host defense. *Nat. Immunol.* 17: 1037–1045.
13. Mills, E. L., B. Kelly, A. Logan, A. S. H. Costa, M. Varma, C. E. Bryant, P. Tourlomousis, J. H. M. Däbritz, E. Gottlieb, I. Latorre, et al. 2016. Succinate dehydrogenase supports metabolic repurposing of mitochondria to drive inflammatory macrophages. *Cell* 167: 457–470.e13.
14. Huang, L., E. V. Nazarova, S. Tan, Y. Liu, and D. G. Russell. 2018. Growth of *Mycobacterium tuberculosis* in vivo segregates with host macrophage metabolism and ontogeny. *J. Exp. Med.* 215: 1135–1152.
15. Mould, K. J., L. Barthel, M. P. Mohning, S. M. Thomas, A. L. McCubbrey, T. Danhorn, S. M. Leach, T. E. Fingerlin, B. P. O'Connor, J. A. Reisz, et al. 2017. Cell origin dictates programming of resident versus recruited macrophages during acute lung injury. *Am. J. Respir. Cell Mol. Biol.* 57: 294–306.
16. Pisu, D., L. Huang, J.K. Grenier, and D.G. Russell. 2020. Dual RNA-Seq of Mtb-infected macrophages in vivo reveals ontologically distinct host-pathogen interactions. *Cell Rep.* 30: 335–350.e4.
17. Mischler, S. E., E. G. Cauda, M. Di Giuseppe, and L. A. Ortiz. 2013. A multicyclone sampling array for the collection of size-segregated occupational aerosols. *J. Occup. Environ. Hyg.* 10: 685–693.
18. Gambelli, F., P. Di, X. Niu, M. Friedman, T. Hammond, D. W. Riches, and L. A. Ortiz. 2004. Phosphorylation of tumor necrosis factor receptor 1 (p55) protects macrophages from silica-induced apoptosis. *J. Biol. Chem.* 279: 2020–2029.
19. Alves, T. C., R. L. Pongratz, X. Zhao, O. Yarborough, S. Sereda, O. Shirihai, G. W. Cline, G. Mason, and R. G. Kibbey. 2015. Integrated, step-wise, mass-isotopomeric flux analysis of the TCA Cycle. *Cell Metab.* 22: 936–947.
20. Mckenzie, M., and M. T. Ryan. 2010. Assembly factors of human mitochondrial complex I and their defects in disease. *IUBMB Life* 62: 497–502.
21. Guerrero-Castillo, S., F. Baertling, D. Kownatzki, H. J. Wessels, S. Arnold, U. Brandt, and L. Nijtmans. 2017. The assembly pathway of mitochondrial respiratory chain complex I. *Cell Metab.* 25: 128–139.
22. Nouws, J., L. G. Nijtmans, J. A. Smeitink, and R. O. Vogel. 2012. Assembly factors as a new class of disease genes for mitochondrial complex I deficiency: cause, pathology and treatment options. *Brain* 135: 12–22.
23. Carneiro, F. R. G., A. Lepelley, J. J. Seeley, M. S. Hayden, and S. Ghosh. 2018. An essential role for ECSIT in mitochondrial complex I assembly and mitophagy in macrophages. *Cell Rep.* 22: 2654–2666.
24. Fazzi, F., J. Njah, M. Di Giuseppe, D.E. Winnica, K. Go, E. Sala, C.M. St Croix, S.C. Watkins, V.A. Tyurin, D.G. Phinney, et al. 2014. TNFR1/phox interaction and TNFR1 mitochondrial translocation Thwart silica-induced pulmonary fibrosis. *J. Immunol.* 192: 3837–3846.
25. Infantino, V., P. Convertini, L. Cucci, M. A. Panaro, M. A. Di Noia, R. Calvello, F. Palmieri, and V. Iacobazzi. 2011. The mitochondrial citrate carrier: a new player in inflammation. *Biochem. J.* 438: 433–436.
26. O'Neill, L. A. 2011. A critical role for citrate metabolism in LPS signalling. *Biochem. J.* 438: e5–e6.
27. Mills, E. L., and L. A. O'Neill. 2016. Reprogramming mitochondrial metabolism in macrophages as an anti-inflammatory signal. *Eur. J. Immunol.* 46: 13–21.
28. Angajala, A., S. Lim, J. B. Phillips, J. H. Kim, C. Yates, Z. You, and M. Tan. 2018. Diverse roles of mitochondria in immune responses: novel insights Into immuno-metabolism. *Front. Immunol.* 9: 1605.
29. Mills, E. L., B. Kelly, and L. A. J. O'Neill. 2017. Mitochondria are the powerhouses of immunity. *Nat. Immunol.* 18: 488–498.
30. Hornung, V., F. Bauernfeind, A. Halle, E. O. Samstad, H. Kono, K. L. Rock, K. A. Fitzgerald, and E. Latz. 2008. Silica crystals and aluminum salts activate the NALP3 inflammasome through phagosomal destabilization. *Nat. Immunol.* 9: 847–856.
31. Corcoran, S. E., and L. A. O'Neill. 2016. HIF1α and metabolic reprogramming in inflammation. *J. Clin. Invest.* 126: 3699–3707.
32. Mills, E., and L. A. O'Neill. 2014. Succinate: a metabolic signal in inflammation. *Trends Cell Biol.* 24: 313–320.
33. Galván-Peña, S., R. G. Carroll, C. Newman, E. C. Hinchy, E. Palsson-McDermott, E. K. Robinson, S. Covarrubias, A. Nadin, A. M. James, M. Haneklaus, et al. 2019. Malonylation of GAPDH is an inflammatory signal in macrophages. *Nat. Commun.* 10: 338.
34. Mills, E. L., D. G. Ryan, H. A. Prag, D. Dikovskaya, D. Menon, Z. Zaslona, M. P. Jedrychowski, A. S. H. Costa, M. Higgins, E. Hams, et al. 2018. Itaconate is an anti-inflammatory metabolite that activates Nrf2 via alkylation of KEAP1. *Nature* 556: 113–117.
35. Lampropoulou, V., A. Sergushichev, M. Bambouskova, S. Nair, E. E. Vincent, E. Loginicheva, L. Cervantes-Barragan, X. Ma, S. C. Huang, T. Griss, et al. 2016. Itaconate links inhibition of succinate dehydrogenase with macrophage metabolic remodeling and regulation of inflammation. *Cell Metab.* 24: 158–166.
36. Warburg, O., F. Wind, and E. Negelein. 1927. The metabolism of tumors in the body. *J. Gen. Physiol.* 8: 519–530.
37. Vogel, R. O., R. J. Janssen, M. A. van den Brand, C. E. Dieteren, S. Verkaart, W. J. Koopman, P. H. Willems, W. Pluk, L. P. van den Heuvel, J. A. Smeitink, and L. G. Nijtmans. 2007. Cytosolic signaling protein Ecsit also localizes to mitochondria where it interacts with chaperone NDUFAF1 and functions in complex I assembly. *Genes Dev.* 21: 615–624.
38. West, A. P., I. E. Brodsky, C. Rahner, D. K. Woo, H. Erdjument-Bromage, P. Tempst, M. C. Walsh, Y. Choi, G. S. Shadel, and S. Ghosh. 2011. TLR signalling augments macrophage bactericidal activity through mitochondrial ROS. *Nature* 472: 476–480.
39. Dostert, C., V. Pétrilli, R. Van Bruggen, C. Steele, B. T. Mossman, and J. Tschopp. 2008. Innate immune activation through Nalp3 inflammasome sensing of asbestos and silica. *Science* 320: 674–677.
40. Piguet, P. F., and C. Vesin. 1994. Treatment by human recombinant soluble TNF receptor of pulmonary fibrosis induced by bleomycin or silica in mice. *Eur. Respir. J.* 7: 515–518.
41. Galván-Peña, S., and L. A. O'Neill. 2014. Metabolic reprograming in macrophage polarization. *Front. Immunol.* 5: 420.
42. Meiser, J., L. Krämer, S. C. Sapcariu, N. Battello, J. Ghelfi, A. F. D'Herouel, A. Skupin, and K. Hiller. 2016. Pro-inflammatory macrophages sustain pyruvate oxidation through pyruvate dehydrogenase for the synthesis of itaconate and to enable cytokine expression. *J. Biol. Chem.* 291: 3932–3946.
43. White, M. R., and E. D. Garcin. 2016. The sweet side of RNA regulation: glyceraldehyde-3-phosphate dehydrogenase as a noncanonical RNA-binding protein. *Wiley Interdiscip. Rev. RNA* 7: 53–70.
44. Scarfì, S., M. Magnone, C. Ferraris, M. Pozzolini, F. Benvenuto, U. Benatti, and M. Giovine. 2009. Ascorbic acid pre-treated quartz stimulates TNF-alpha release in RAW 264.7 murine macrophages through ROS production and membrane lipid peroxidation. *Respir. Res.* 10: 25.
45. Naik, E., and V. M. Dixit. 2011. Mitochondrial reactive oxygen species drive proinflammatory cytokine production. *J. Exp. Med.* 208: 417–420.
46. Michelucci, A., T. Cordes, J. Ghelfi, A. Pailot, N. Reiling, O. Goldmann, T. Binz, A. Wegner, A. Tallam, A. Rausell, et al. 2013. Immune-responsive gene 1 protein links metabolism to immunity by catalyzing itaconic acid production. *Proc. Natl. Acad. Sci. USA* 110: 7820–7825.
47. Cordes, T., M. Wallace, A. Michelucci, A. S. Divakaruni, S. C. Sapcariu, C. Sousa, H. Koseki, P. Cabrales, A. N. Murphy, K. Hiller, and C. M. Metallo. 2016. Immunoresponsive gene 1 and itaconate inhibit succinate dehydrogenase to modulate intracellular succinate levels. *J. Biol. Chem.* 291: 14274–14284.
48. Phinney, D. G., M. Di Giuseppe, J. Njah, E. Sala, S. Shiva, C. M. St Croix, D. B. Stolz, S. C. Watkins, Y. P. Di, G. D. Leikauf, et al. 2015. Mesenchymal stem cells use extracellular vesicles to outsource mitophagy and shuttle microRNAs. *Nat. Commun.* 6: 8472.